Coherence Effects in Higgs Boson Production via Weak Boson Fusion at the LHC - A Comparative Study

Shay Alexander Payne

Student ID: 27760812

Supervisor:

Professor Peter Skands

A thesis presented for the degree of
Bachelor of Science (Honours)

School of Physics and Astronomy
Faculty of Science
Monash University
Australia

December 4, 2020

Abstract

Physicists are currently studying the Higgs Boson at the Large Hadron Collider in hope that it will lead to hints toward physics beyond the Standard Model. However, there is indication that coherence effects are not faithfully reproduced with regards to radiative corrections in the Higgs production channel Weak Boson Fusion, via traditional event generator showers; whereas these effects are reproduced in a more modern formalism, the antenna/dipole shower. In this thesis we test these two models on Weak Boson Fusion: a traditional parton shower model as simulated by PYTHIA and an antenna shower model as simulated by VINCIA. We find that there are significant differences between these two models with regards to observables known to be sensitive to this coherence, with PYTHIA overestimating the amount of radiation we expect to see.

Acknowledgments

Wow ,what a year it has been. Honours, in the best of times, is a great challenge. With the onset of a global pandemic this has not been made any easier! Even so, with the help of the many people listed here (along with my lovely home espresso machine) I have made it - I hope this thesis reflects the many long days it has taken to get there.

First and foremost I must thank my supervisor Professor Peter Skands, whose seemingly infinite wisdom on all things QCD has brought this thesis in to what I hope is a *coherent* state. Despite not even being able to use a whiteboard to explain the many concepts necessary to have a grasp on the fundamentals of QDC phenomenology, Peter has guided me well throughout the year. I can not express enough my gratitude to you for your guidance throughout honours, I could not have asked for a more thorough and understanding supervisor for honours, thank you.

Secondly I must thank Peter's PhD student Christian Preuss. Taking an interest in my project your help and guidance this year has been immeasurable. From allowing my to produce real scientific level plots to giving us hints into what the NLO+LL WBF phenomena will be, my project would be a shadow of what it is currently without your help. I hope after after my thesis is submitted you can get a well deserved sleep in after your many days of waking up at 6 in the morning for the sake of my work! Thank you.

Next I want to thank my fellow honours cohort. I would be lying if I said that in this year we did not at times feel very distant from each over, however many other times I felt closer than ever to my fellow students. I wish you all the best for your own thesis's, and for the future ahead of you.

I wish to thank those closest to me this year my family - both biological and those who have chosen to live with me (what whatever crazy reason). I thank you all for tolerating me this year during honours, and for your lending me your ears when listening to me during my thesis. I know it must be a struggle hearing me talk about my thesis for the 50'th time, thankfully it is all over now.

Lastly I wish to give special thanks to my cat Black Cat. You're faithful companionship throughout my honours, and particularly during lockdown, is probably the only reason I was about to finish this thesis in the first place. I love you and will treasure you always. Thank you.

Contents

Chapter 1

Introduction

Ever since its original formulation in the 1960s [1–3] the Higgs mechanism, and hence the Higgs Boson has been an elusive particle. It wasn't until 2012 when physicists at CERN discovered the Higgs Boson at the Large Hadron Collider (LHC) with the use of the ATLAS and CMS detectors [4, 5]. With this discovery the final piece of the Standard Model was complete; the Higgs Boson, with its now known mass of approximately 125 GeV stands as one of the finest testaments to the predictive power of the Standard Model.

However, we know the Standard Model is not complete. It makes no mention of the possible origins of dark matter, a mysterious substance which is thought to interact with only the gravitational force, and is believed to constitute the majority of matter in the universe [6]. It also makes no real predictions about dark energy, which is believed to constitute a majority of the energy in the universe [6]. As such the Standard Model only predicts approximately 5% of the mass/energy which is believed to exist, which is a major shortfall.

This is only the beginning, for example the Standard Model by definition is incomplete: only including the strong (QCD/colour force), electrodynamic and weak forces while excluding descriptions of the gravitational force. Given this context, searches for Beyond Standard Model (BSM) physics is of great importance to modern physics. This brings us back to the Higgs, as the newest discovered particle of the Standard Model it is consequentially the least probed, as such there is great potential for discrepancies to appear between Standard Model predictions of the Higgs and experimental realities. Furthermore the Higgs Boson, and its underlying quantum field the Higgs field, is fundamentally linked to a large portion of the Standard Model. As such many BSM theories rely on modified Higgs parameters to be successful and studies of Higgs physics are popular in both experimental and theoretical high energy particle physics.

One of the popular Higgs production channels to study at the LHC is known as Weak Boson Fusion (WBF). This process creates a Higgs boson via either two $W^{\pm}$ or Z bosons, gauge bosons of the weak force. These in turn are both emitted from scattered quarks, particles primarily associated with the strong force[1] (QCD), which reside within protons. Furthermore, WBF produces two characteristic hard (high energy) QCD jets, bundles of particles grouped together in cone like structures, from the scattered quarks in this interaction. These jets are detected in the forwards and backwards regions of the detectors at the LHC, with the produced Higgs being located at central regions of rapidity. Due to the structure of the QCD radiation pattern produced by this processes, coherent

---

[1]Though quarks do have both QED, QCD and weak charge - hence interacting with all forces of the Standard Model

suppression of this radiation occurs in this central rapidity region, right where the Higgs is produced. As such we are left with a rather "clean" signal to detect the Higgs decay products, making WBF well suited for experimental studies.

Of course we want to be able to make predictions for, and comparisons against these experimental results. As such significant research in the field of QCD phenomenology is dedicated towards accurate simulations of high energy particle physics using what are known as event generators. These processes, just like experimental results at the LHC, are dominated by QCD and its radiative corrections via gluon radiation. Important for these processes is the concept of coherence, in particular of coherence with respect to QCD radiation. This coherent radiation can be thought of physically in terms of radiating particles. Incoming and outgoing particles in an interaction at the LHC both emit large amounts of QCD bremßralung radiation as they are scattered. Naively one could consider the radiation of both particles independently, leading to an incoherent treatment of radiation. However this incoherent approach does not capture the correct physics - if one instead treats the radiating particles as a QCD colour-dipole instead (analogous to a electromagnetic dipole) we reproduce a coherent pattern of radiation, which is exactly what we see in collider events at the LHC.

Accurate descriptions of this colour coherence depend highly on the so called shower model used in an event generator. Traditional approaches (DGLAP showers) use a shower model which is *a priori* incoherent, as such other techniques must be used to bring back radiative coherence using this model. These techniques, so far, have been effective, however it has been theorised that for processes with similar radiation patterns to WBF that these techniques break down. An alternative approach known as an antenna shower, which be contrast *is* inherently coherent. As such if the assumption that coherence is not accurately simulated for WBF in traditional event generators then a straightforward way to test for this would be to compare two of these such different models to each over, and observe any differences apparent in how they treat coherent radiation.

For my project I compare the treatment of coherence on Higgs production via WBF at the LHC to LO+shower[2] accuracy using the PYTHIA (a DGLAP based shower) and VINCIA (an antenna shower shower). The results of this thesis should demonstrate that a inherently coherent treatment of WBF is needed for LO+LL accuracy if one wishes to accurately simulate phenomena associated with WBF. Beginning in chapter 2 we discuss the background physics of this project, discussing the importance of coherence in modern particle physics; as well as discussing the Higgs and it's importance in the standard model andl as why Weak Boson fusion is an important Higgs production channel for study. In chapter 3 we discuss the more of the technical details of the event generators we use and the parton showers models they employ, as well as how coherence is faithfully reproduced using these models. Chapter 4 deals with some of the technicalities of the shower generation, as well as some of the specific language used in QCD phenomenology/experimental particle physics, with Chapter 5 detailing the results of our analysis and chapter 6 listing our final conclusions and thoughts for further analysis.

---

[2]Which we will see in section 3 is typically referred to as LO+LL (Leading Logarithm)

Chapter 2

Background Theory

2.1   Quantum Coherence

The property of coherence has been known to physics for centuries; classically coherence is considered to be a fundamental property of waves, with two wave sources considered to be perfectly coherent when their phase difference is constant and their frequency and waveform are the same. In this sense, processes embody coherence when we are sensitive to the coherent sum of waves, and incoherent when we do not need to consider this coherent sum.

From this classical description of coherence we naturally transition towards a quantum description. In quantum mechanics all objects have some wave-particle duality, as such it is not surprising that coherence is a fundamental property of objects in quantum mechanics. Even fundamental particles, such as photons or electrons, experience coherent behavior; this was famously demonstrated by modifying the Young double slit experiment to only allow one photon/electron at a time to enter the slit. Even with only one particle at a time coherent behavior is still observed [7, 8].
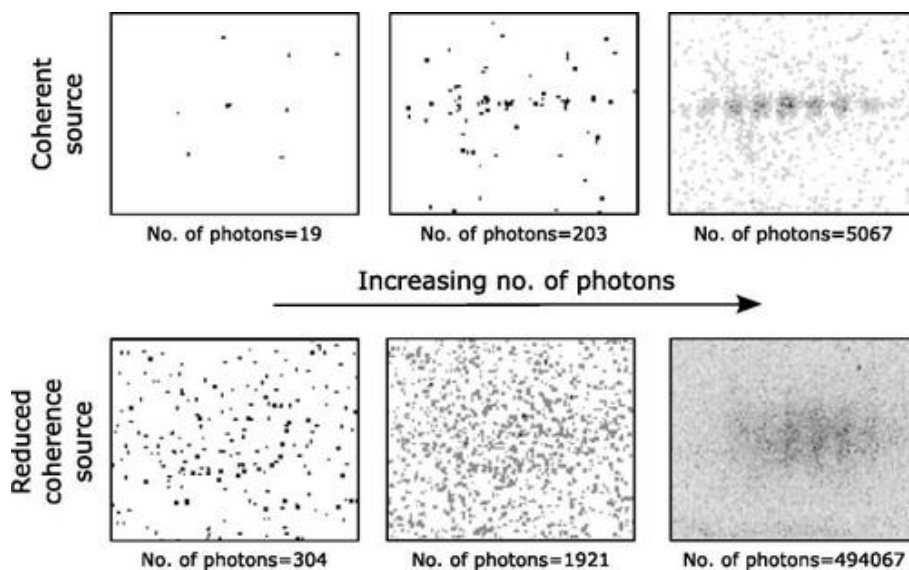
Figure 2.1: The double slit experiment one photon at a time using coherent and incoherent incoming light. As can be seen while individual photons might appear to be moving through the slits at random, as the photon number increases the coherent nature of quantum particles becomes apparent [7].

3

Quantum coherence manifests itself in many ways, a straightforward example of quantum coherence is interference terms that often appear in between Feynman diagrams describing a quantum system to a fixed order in perturbation theory.

2.1.1 The Chudakov effect - angular ordering of coherent radiation

Unsurprisingly particle physics, which is built on the framework of quantum field theory - a relativistic quantum theory, is rich with coherent processes. One of the earlier examples of coherence in the context of particle physics is the so called "Chudakov" effect. The Chudakov effect, discovered by Soviet physicist Aleksandr Evgenievich Chudakov [9], is an archetypal example of coherence in QED radiation (which, as we will see, generalises to QCD radiation). In 1955 Aleksandr Chudakov was working on the effects of ionisation due to electron positron pairs created by cosmic rays hitting atoms in an emulsion plate. He found that the ionisation, which is caused by the emission of gamma rays from the electron/positron, was suppressed until the electron positron pair was further separated. The basic experimental set-up is shown in figure 2.2:
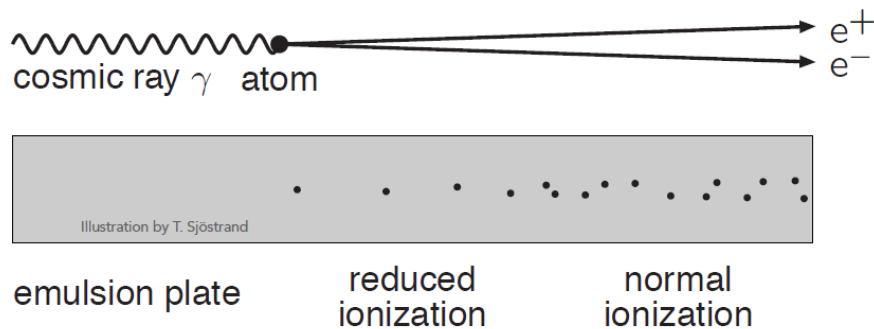
Figure 2.2: A basic diagram illustrating the Chudakov effect. A cosmic ray hits an atom which causes an electron positron pair [10].

The basic idea behind the Chudakov effect is that photons with long wavelength can not differentiate between the electron and positron (which act as a closely bound QED dipole), as such the photon sees an electrically neutral object and hence its emission is suppressed.

The Chudakov effect is fascinating enough that I believe that it will be constructive to go through the mathematics of where the suppression of ionisation comes from, which can be explained simply using time-ordered (old-fashioned) perturbation theory [11]. Take the Feynman diagram shown below:
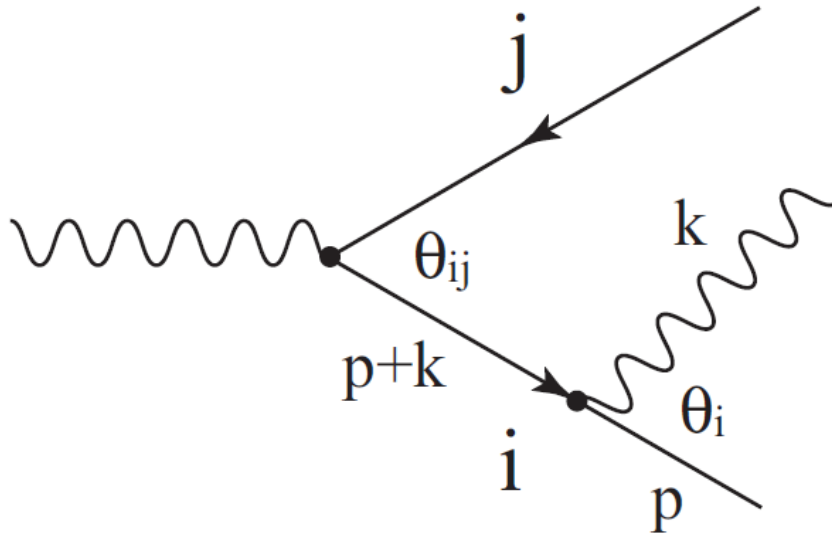
Figure 2.3: Feynman diagram for e^+ e^- pair production via gamma rays with a later ionising radiation emission coming from one of the electron positron pairs. The electron is labeled i and the positron is labeled j [11].

In time ordered perturbation theory the energy difference between the electron in the virtual (with momentum $\mathbf{p} + \mathbf{k}$) and final (with momentum $\mathbf{p}$) state, in the soft photon limit where $|\mathbf{k}| \ll |\mathbf{p}|$ and where the angle θ_i, is:

$$\Delta E = \sqrt{\mathbf{p}^2 + m^2} + |\mathbf{k}|\sqrt{(\mathbf{p} + \mathbf{k})^2 + m^2} \sim |\mathbf{k}|\theta_i^2. \tag{2.1}$$

We have from Heisenberg's uncertainty principle that (in natural units):

$$\Delta E \Delta t \sim 1. \tag{2.2}$$

Which means that we have:

$$\Delta t \sim \frac{1}{|\mathbf{k}|\theta_i^2} \sim \frac{\lambda}{\theta_i} \tag{2.3}$$

Now during the time interval Δt the separation between electron and positron Δd becomes:

$$\Delta d \sim \Delta t \theta_{ij} \sim \lambda \frac{\theta_{ij}}{\theta_i}, \tag{2.4}$$

where we have substituted in the previously calculated quantity for Δt. Now it is clear when this suppression occurs, if $\Delta d < \lambda$, the photon can't distinguish the separation of the electron positron pair, hence the production of a photon is suppressed. Furthermore this suppression depends on the angle of emission θ_i, with large angles leading to further suppression of soft photons.

This angular ordering property, that is, that soft photons are suppressed as a function of their opening angle, generalises to QCD radiation and is the basis for radiative coherence that occurs for high energy events at colliders such as the Large Hadron Collider. As such, if one wishes to simulate the radiative corrections to fixed-order predictions in perturbation theory this angular ordering property will need to be considered to generate an accurate picture of the process in consideration.

2.1.2 Colour Dipoles

When considering coherent QCD radiation from a particle the first possibility that can be used is to treat the particle independently of others and simply consider $1 \to 2$ kinematics for the creation of radiation. This approach can be made to work, though as we'll see in section 3.2 of this thesis there are some caveats, such as the violation of energy and momentum in this approach and the fact that we have to reintroduce the angular ordering of radiation (as seen in the Chudakov effect) through other methods. An alternative, and more physical approach is instead of treating the system as the incoherent sum of monopoles we can treat them as the sum of systems of two-particle QCD colour"dipoles" using $2 \to 3$ kinematics for radiation instead. This approach offers a more accurate description of the radiation kinematics and is somewhat analogous to the multipole expansion in QED, where we have moved from a "monopole" to "dipole" treatment. As we'll see, these colour dipoles are the main source of coherence for QCD bremßtralung, which is the dominant form of radiation for Weak Boson Fusion. One should be careful, however, about how they conceptualize this concept. For example the largest contribution from WBF is the dipole formed by the scattered quarks (see section 2.2.3 for a kinematical description of this process). This leads to a dipole forming between the initial quark before scattering, and the final quark after scattering. As such these dipoles are formed across a time separation, as opposed to being separated in space, creating coherence in a way somewhat reminiscent of the double slit experiment.

2.2 Higgs Physics

2.2.1 The Need for the Higgs in the Standard Model

The basis of modern particle physics is quantum field theory. In it, we can describe electrodynamics, the strong and the weak force in terms of fundamental fields, parametrised by their Lagrangian. To explain why a Higgs field is needed to complete the Standard Model let's consider the simplest Lagrangian, the quantum electrodynamic (QED) Lagrangian for interactions between the electron and a massless photon. This is given by:

$$\mathcal{L}_{\text{QED}} = \bar{\psi}(i\gamma^\mu \partial_\mu - m_e)\psi + e\bar{\psi}\gamma^\mu A_\mu \psi - \frac{1}{4}F_{\mu\nu}F^{\mu\nu}, \tag{2.5}$$

where A_μ is the electrodynamic 4-potential, m_e is the electron mass, ψ and $\bar{\psi}$ are the Dirac and Dirac adjoint spinors respectively, γ^μ is the gamma matrix and $F^{\mu\nu}$ is the electromagnetic field strength tensor. Importantly, just like in classical electrodynamics the QED Lagrangian satisfies U(1) local gauge invariance, that is, we can apply the transformation:

$$A_\mu \to A'_\mu = A_\mu - \partial_\mu \chi, \tag{2.6}$$

for some arbitrary scalar field χ and retain the same Lagrangian. If we instead wanted to consider a massive photon of mass m_γ we would be required to add a term of $\frac{1}{2}m_\gamma^2 A_\mu A^\mu$ to our Lagrangian. Which gives:

$$\mathcal{L}_{\text{QED}} = \bar{\psi}(i\gamma^\mu \partial_\mu - m_e)\psi + e\bar{\psi}\gamma^\mu A_\mu \psi - \frac{1}{4}F_{\mu\nu}F^{\mu\nu} + \frac{1}{2}m_\gamma^2 A_\mu A^\mu. \tag{2.7}$$

If we apply the transformation $A_\mu \to A'_\mu = A_\mu - \partial_\mu \chi$ to our additional terms we have:

$$\frac{1}{2}m_\gamma^2 A_\mu A^\mu \to \frac{1}{2}m_\gamma^2 (A_\mu - \partial_\mu \chi)(A^\mu - \partial^\mu \chi) \neq \frac{1}{2}m_\gamma^2 A_\mu A^\mu. \tag{2.8}$$

As such the addition of a mass term for the gauge boson of QED, the photon, has broken the local gauge invariance of QED!

We know that the photon is in fact massless, as is the gauge boson for QCD, the gluon. However the two gauge bosons for the weak force the W and Z bosons are known to be massive. We expect that QED, weak force and QCD to obey U(1), $SU(2)_L$ and $SU(3)$ local gauge invariance respectively[1]. As such, we can't explain the masses of the gauge bosons in the weak sector as some kind of inherent mass, they must be the result of some "unknown phenomena". Similarly, it turns out that fermion masses too can not be explained without this addition. As we will see this missing "unknown phenomena" is the Higgs field, whose corresponding quantum excitation is the Higgs boson.
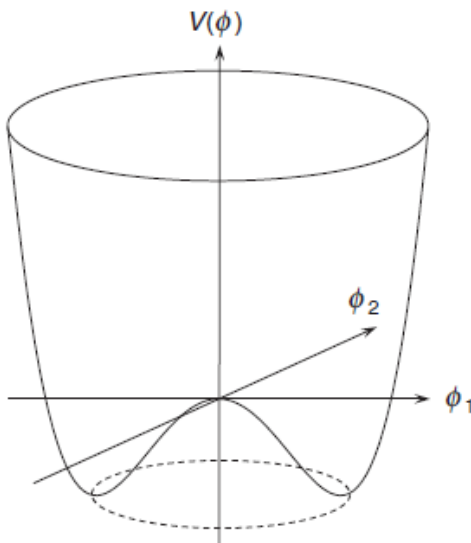
Figure 2.4: The so called "Mexican hat" potential, named after its sombrero-like shape. [12].

The solution to the mass problem in the Standard Model was solved independently by three groups in the 1960s [1–3], though ultimately it was Higgs who was has been most famously remembered for the solution. The Higgs mechanism involves the addition of a complex doublet scalar field known as the Higgs field:

$$\phi = \begin{pmatrix} \phi^+ \\ \phi^0 \end{pmatrix} = \frac{1}{\sqrt{2}} \begin{pmatrix} \phi_1 + i\phi_2 \\ \phi_3 + i\phi_4 \end{pmatrix} \tag{2.9}$$

This field has an associated Lagrangian given by:

$$\mathcal{L}_{\text{Higgs}} = (\partial_\mu \phi)^\dagger (\partial^\mu \phi) - V(\phi), \tag{2.10}$$

where $V(\phi)$ is the Higgs potential, given by:

$$V(\phi) = \mu^2 \phi^\dagger \phi + \lambda (\phi^\dagger \phi)^2, \tag{2.11}$$

where μ^2 and λ are free parameters. $\lambda > 0$ is required to give a finite minimum for the potential, while $\mu^2 < 0$ gives an infinite set of minima which, importantly, do not lie

---

[1]and by extension the combined $SU(2) \times U(1)_Y$ local gauge invariance of the unified electroweak sector

on the zero point of the field. This form of the potential is colloquially known as the "Mexican hat" potential, shown in figure 2.4.

This change from the 0 point in the Higgs field to the ground/vacuum state (for which the most common choice is $\phi_1 = \phi_2 = \phi_4 = 0$ and $\phi_3 = v$, known as the unitary gauge) breaks the $\mathrm{SU}(2)_L \times \mathrm{U}(1)_Y$ symmetry of the electroweak force, while leaving the $\mathrm{U}(1)$ QED symmetry unbroken. This leads to a prediction of the W and Z masses of:

$$m_W = \frac{1}{2} g_W v \tag{2.12}$$

$$m_Z = \frac{1}{2} v \sqrt{g_W^2 + g'^2}, \tag{2.13}$$

where v is the Higgs vacuum expectation value and g_W and g' are the $\mathrm{SU}(2)_L$ and $\mathrm{U}(1)$ gauge coupling constants respectively. These masses can further be related to each over by the following relation:

$$m_Z = \frac{m_W}{cos\theta_W}, \tag{2.14}$$

where θ_W is the weak mixing angle.

The Higgs field also couples to fermions, giving them mass as well. Fermions with larger masses are more strongly coupled to the Higgs field.

The resultant excitation of this field is known as the Higgs boson, it is a scalar, spin-0 boson, with no electric charge or colour charge and can interact with any Standard Model particle with weak charge.

As such, is it apparent why the Higgs boson is so important. It is the main link to the Higgs field, which is responsible for generating the mass of fermions and gauge bosons in the Standard Model. The Higgs boson interacts with particles across the standard model, and has an intricate relationship to the electroweak force due to the symmetry breaking property of the Higgs field. Furthermore, it becomes even more apparent why studying the Higgs is worthwhile when considering the so called free parameters of the Standard Model. The free parameters are constants that are not directly predicted by quantum field theory and thus must be probed experimentally. These act to pin down the expected behaviour within the Standard Model, as by knowing these parameters we should be able to predict everything within the theory. An example of some of the constants is shown in table 2.1.

Parameters of the SM			
Couplings			
Electric charge	$q = \sqrt{4\pi\alpha}$	0.3028221(31)	
Mixing angle	$\sin\theta_W$	0.23122(15)	
Boson masses			
W	m_W	80.385(15)	GeV
Higgs	m_H	40–1600	GeV†
Fermion masses			
Leptons			
e	m_e	510.998928(11)	keV
μ	m_μ	105.6583715(35)	MeV
τ	m_τ	1.77682(16)	GeV
Quarks			
u	m_u	1.7–3.1	MeV
d	m_d	4.1–5.7	MeV
c	m_c	$1.29\pm^{0.05}_{0.11}$	GeV
s	m_s	$0.1\pm^{0.03}_{0.02}$	GeV
t	m_t	173.21(87)	GeV
b	m_b	4.18(3)	GeV
CKM angles and phase			
φ_{12}		13.04(5)	°
φ_{13}		0.201(11)	°
φ_{23}		2.38(6)	°
δ_{13}		1.20(8)	rad

Table 2.1: Free parameters of the Standard Model in the electroweak sector. All except the electric charge are related to the Higgs boson. [13]

With the discovery of the Higgs Boson by the ATLAS and CMS detectors at the LHC [4, 5] along with the measurement of its mass, one of the last remaining free parameters was finally known (though precision measurements of other free parameters are still ongoing [14]). As such we have firm theoretical predictions as to how we expect Standard Model particles to behave. The Higgs Boson, being the last particle discovered in the Standard Model, is consequentially one of the least probed experimentally. As such any behavior of the Higgs found that does not fit the Standard Model and its parameters may point physicists in the direction of BSM physics.

2.2.2   Higgs Phenomenology in Particle Colliders

While the theoretical basis of the Higgs Boson was proposed in the 60s the experimental verification of the Higgs mass, and hence the Higgs Boson, would take decades longer; as a free parameter of the Standard Model the mass of the Higgs was an open problem. Early attempts to constrain the Higgs Boson mass used electroweak precision measurements, which implied that the Higgs mass should be less than 152GeV at the 95% confidence level [15]. Further measurements at the Large Electron Positron collider (LEP) gave a lower bound of >114 GeV at 95% confidence [16], while the Tetravon excluded the 162–166 GeV mass range with 95% confidence [17], with the Tetravon further indicating the Higgs likely lies within the mass range of 120-135 GeV [18]. With the discovery of the Higgs at the LHC in 2012, its mass was finally measured to be approximately 125 GeV [4, 5]. With this known the remaining main areas of study for the Higgs are determination of the Higgs spin (to see if it is inline with SM predictions) and how it interacts with other SM

(and BSM) particles, which can be categorised into Higgs production and Higgs decay.

Higgs Boson Production

As the mass of the gauge bosons and fermions are generated by the Higgs field it is not surprising that the Higgs boson is more strongly coupled to massive particles. In contrast the LHC uses proton proton beams for particle collisions; where protons can be considered to be made up mostly of massless gluons and light quarks [19]. As such the dominant production modes at the LHC involve light or massless particles.
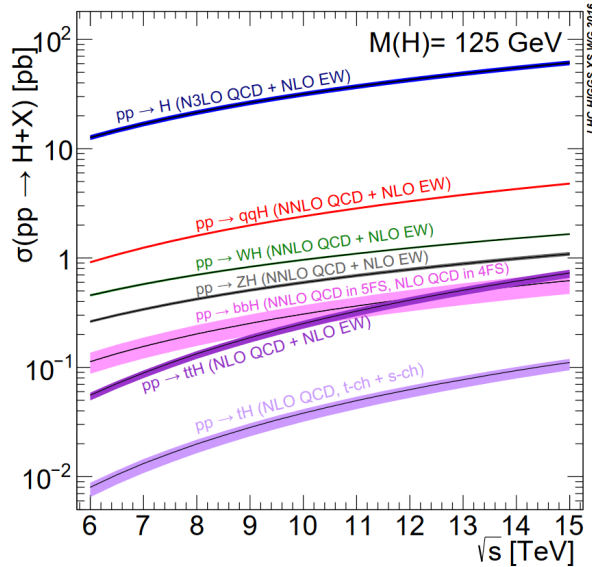
Figure 2.5: Production cross sections for SM Higgs at the LHC as a function of the centre-of-mass energy, $\sqrt{s}$, of the incoming beam. The shorthand $pp \rightarrow H$ is gluon-gluon fusion, while $pp \rightarrow qqH$ is Weak Boson Fusion and $pp \rightarrow WH/ZH$ is Higgs-strahlung [20].

Looking at figure 2.5 the dominant form of Higgs production at the LHC is gluon-gluon (gg) fusion. Gluons can not directly couple to the Higgs (hence why they are massless), and must instead form a virtual quark loop. This quark loop is typically made of top quarks, the heaviest quark, however bottom quarks also make a noticeable contribution to the production cross section for gluon-gluon fusion [21]. While it is the dominant production mode for the Higgs it also suffers from large theoretical uncertainties of order $\mathcal{O}(10 - 20\%)$ even with NNLO (next-to-next-to leading order) QCD corrections included [22]. Gluon-gluon fusion is not as well identifiable compared to typical QCD background processes, as such other production modes are often also considered when studying the Higgs.
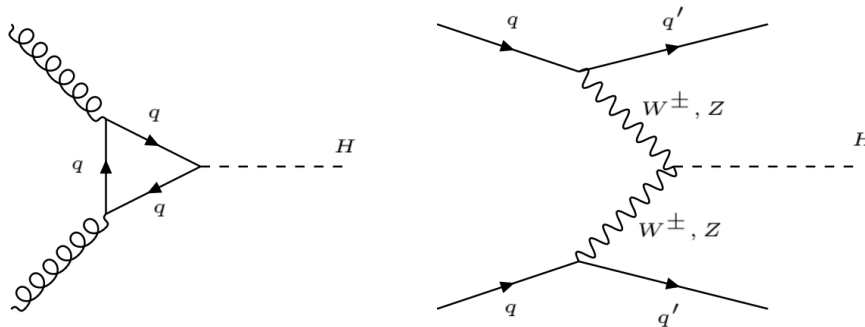
Figure 2.6: Feynman diagrams for gluon gluon fusion (left) and weak boson fusion (right).

The second most dominant production mechanism for the Higgs is Weak Boson Fusion (WBF, also known as Vector Boson Fusion, VBF) and has a production cross section $\mathcal{O}(10)$ times smaller than gluon-gluon fusion. Early studies indicated it as the dominant form of Higgs production for a heavy Higgs with $m_H > 6m_W$ [23], where m_W is the W Boson mass. This would turn out not to be the case as the SM Higgs has a mass of $m_H \sim 1.5\, m_W$, even so WBF is well suited as a contender to study Higgs processes. This is partly due to the identifiable nature of the process: WBF produces two characteristic "tagging" QCD jets from the two scattered quarks in the process, with these jets being hard (high energy) and produced back-to-back in the forward and backward regions of the detector [24]. This allows for easier detection of the WBF jets compared to what one would naively expect due to its smaller cross section. Furthermore, due to the colour-singlet nature of weak boson exchange in WBF gluon radiation is suppressed in regions of central rapidity, as opposed to background processes (and other channels of Higgs production such as gluon-gluon fusion which induce stronger QCD radiative effects in this region). These properties of WBF Higgs production can be used to extract its signal from typically quite large QCD background processes. WBF also has the advantage that there are simple "benchmark" processes that it can be compared to, that is, Z and W boson production via WBF. Z and W boson production contain many of the same features of Higgs Boson production, such as the forward and backward "tagging" jets and QCD suppression in central rapidity regions - in particular single Z production via WBF is very similar to Higgs production via WBF [25]. The production cross sections for WBF Z and W production are higher than for Higgs production, and are thus well suited to precision measurements to benchmark the Higgs production process. This is an active area of study, with recent results from the ATLAS detector at the LHC being published as recently as 2019 [26]. Important to note is that enhancements in WBF cross sections are indicators of BSM physics [27], and as such are drivers for interest in the Higgs WBF production channel.

Some mention should also be given to the sub-leading production processes at the LHC. The most important of which is Higgs-strahlung. This process has the advantage that it can be relatively "clean", as the final W/Z boson can decay purely leptonically, avoiding much of the complicated QCD jet structure other processes generate in final state particle decays. In particular, Higgs-strahlung is well suited to studies of Higgs decays into $b\bar{b}$ quark pairs to detect the clear signal [28], however the relatively small production cross section for this sub-leading process makes studying this process challenging.

Higgs Boson Decay

The Higgs boson is an unstable particle with lifetime of $\mathcal{O}(10^{-22})$ seconds. As such we can not detect the Higgs itself at the LHC and must rely on detecting the remnants of Higgs decays.
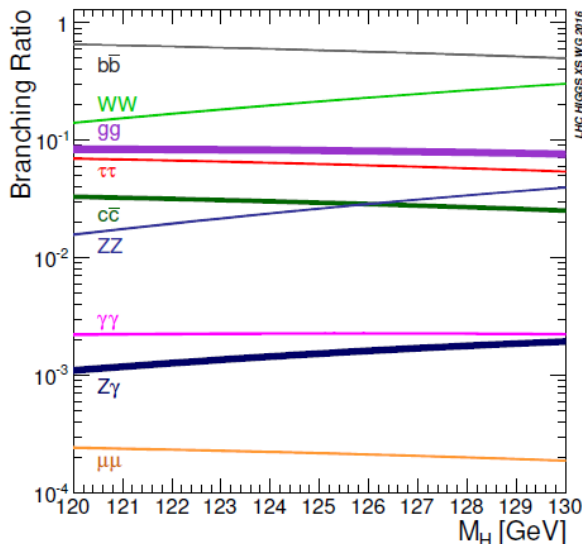
Figure 2.7: Branching ratios for the Higgs boson with mass around 125 GeV [29].

As the Higgs couples to heavy particles more strongly it is not surprising that the largest branching ratio is $H \rightarrow b\bar{b}$, with the bottom quark being the second heaviest quark[2]. This decay can be detected by using b-tagging to detect jets generated via bottom quarks; with the exception of Higgs-strahlung production, which has a small production cross section at the LHC, this decay channel is difficult to detect due to very large QCD backgrounds (such as $gg \rightarrow b\bar{b}$). So much so that it would take six years after the initial discovery of the Higgs for the Higgs to be detected using this channel [30]. Lastly $H \rightarrow c\bar{c}$ decays are similar to $H \rightarrow b\bar{b}$, with c-tagging used for the jets instead [31].

One of the more important decay channels is the photon-photon decay. While it has a very small branching ratio (the Higgs can not couple directly with photons as they are massless, and must do so through virtual loop corrections) it also has a very clean, identifiable signal. As such this channel was the first that the Higgs was identified in [4, 5].

The other important decay channels to consider are the WW and ZZ channels. These can also give a relativity clean signal, and as such were the next two channels the Higgs was measured in, however these channels are suppressed due to the fact that at least one of the W/Z pairs must be off-shell[3]. Furthermore, these decays only give "clean" detections when both W or Z bosons decay leptonically, and as such the effective branching ratio of these decays when only including leptonic decays are significantly lowered. Even so, these decays give recognisable signals that make them prime candidates for Higgs studies.

---

[2]One might then ask "why is the top not preferred over the bottom quark, as the top quark has a heavier mass?" The answer is that the mass of two top quarks is far greater then the Higgs mass, at 346 GeV, and as such can not produce an on-shell Higgs.

[3]Since $m_H < 2m_W$ and $m_H < 2m_Z$

2.2.3   A closer look at Weak Boson Fusion

Before discussing the simulation of these events with Monte Carlo Event generators (discussed in chapter 3) special attention should be brought to the Weak Boson Fusion production channel, which as the focus of this thesis deserves special attention.

As stated in section 2.2.1 in Higgs Boson production we see coherent suppression in the central rapidity region where the Higgs is located. This can understood intuitively by considering the QCD colour flow in the process as per figure 2.8.
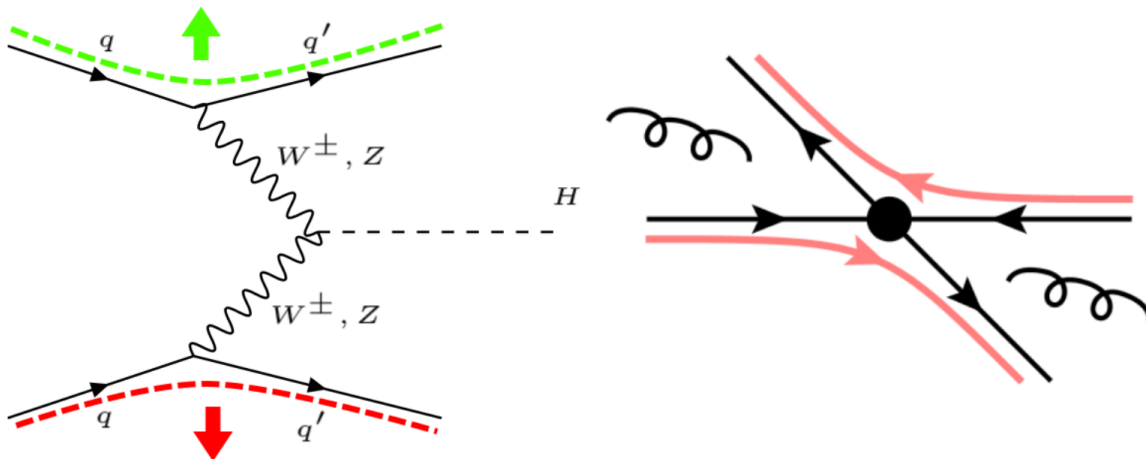
Figure 2.8: QCD colour flow superimposed on Feynman (left) and kinematic (right) diagrams of the LO process [32].

From here it can be seen why we arrive at a coherent suppression in this central region; the incoming/outgoing quarks, which produce QCD bremßtralung when kicked, produce soft radiation in the direction away from the Higgs Boson and towards the beam axis (z direction). All other vertices of the Born level diagram contain no QCD colour and as such do not produce QCD radiation. This leads to no QCD radiation in this central region, while the forwards regions close to the beam axis of the detector contain two noticeable jets; located as such due to the kinematics of the interaction.

This is particularly important for studying the Higgs Boson as the Higgs and its decay products are located in the low rapidity/pseudorapidity regions of the detector. For general purpose detectors such as ATLAS or CMS (both detectors where the Higgs was first discovered) these regions are where the detector is most precise, with individual charged particle tracking abilities within $|\eta| < 2.5$ for ATLAS and $|\eta| < 2.4$ for CMS [33, 34]. Compare this to gluon-gluon fusion in 2.5. In gluon gluon fusion all LO vertices contain QCD colour charge, as such we expect QCD radiation to dominate throughout phase space. That isn't to say that the radiation pattern is directionless, but at the very least it can be said that we do not generate the characteristic QCD coherent suppression that a process such as WBF generates.

It is evident from here then that coherence is vitally important if one wished to describe the features of Weak Boson Fusion. When considering the important experimental features of WBF the most prominent are:

- **Tagging jets**: The most prominent features of this production channel are the two "tagging"/"forward" jets. These are the two QCD jet structures produced by the two scatterd quarks from the LO processes and as such have high jet-jet invariant mass; furthermore as their name suggests are located close to the beam axis, and as such leave a wide range of pseudorapidity for detection of the Higgs decay products.

- **Third jet:** These are any additional jets produced in the pseudorapidity region between the two tagging jets. Since this is the region that QCD coherent suppression occurs we expect this third jet to be particularly sensitive to coherence, and as such is a interesting observable to study if one wishes to study the effects of coherence on WBF, as is the case in this thesis.

- **Higgs decays:** This is a broad category for the decay products of the Higgs, for the case of this thesis I will be considering the Higgs decaying to two photons, as this decay channel produces two hard photons that are easily detected. Other more common decay channels exist however, such as bottom $q\bar{q}$ pairs which can be identified using b-tagging on the resultant QCD jets.

Lastly a discussion of Higgs boson detection via Weak Boson Fusion would be amiss if we did not also mention the background processes for WBF detection. These are processes that mimic the behavior of WBF and are not distinguishable without strategic cuts in phase space.

For example for a Higgs decaying into to two photons a preliminary (and, without any cuts on phase space, naive) analysis with PYTHIA[4] at default settings with $\hat{s} = 13$ TeV gives us relative cross sections for WBF, gluon-gluon fusion and other proton-proton to photon channels of:

$$\sigma_{\text{wbf}} = (6.1 \pm 0.1) \times 10^{-12} \text{ mb}$$
$$\sigma_{\text{gg}} = (5.7 \pm 0.1) \times 10^{-11} \text{ mb} \tag{2.15}$$
$$\sigma_{\text{pp}} = (1.15 \pm 0.02) \times 10^{-4} \text{ mb}$$

As can be seen, gluon-gluon fusion has a cross section on the order of 10 times higher than WBF, while background noise from *pp* collisions are an impressive order of $\approx 10^8$ times higher. Even for more common decay channels of the Higgs the cross section for WBF will always be lower than that of the background processes, and as such we will have to make use of significant cuts to the phase space of the process.

These cuts typically come in the form of cuts to the tagging jets, the third jet and the decay products of the Higgs [35]. For my research see chapter 4 for the specific cuts I will be using for WBF, however in general: for the tagging jets typical cuts include a high jet-jet invariant mass, large separation in pseudorapidity and jets detected in opposite hemispheres. For decay products of the Higgs this is largely specific to the decay channel we are interested in, however a reasonable starting point is to consider events where the decay products have a total invariant mass close to the Higgs mass of 125 GeV. Lastly, we have the third jet veto: this is a condition that, due to the coherent QCD suppression between the two tagging jets, we expect little activity between the two tagging jets (bar decay products of the Higgs) and as such can make a veto on any events containing a third jet while still retaining the majority of our WBF events (while removing a large amount of background events which are not sensitive to any suppression in this region).

---

[4]See chapter 3 on event generators for more information on PYTHIA and other event generators

Implementing these cuts allows us to analyze our WBF data without being overwhelmed by background noise, however this comes at a cost: These cuts significantly reduce the phase space of our event and consequently we are forced to reject some amount of true positives, that is, data that genuinely came from WBF events. This is a necessary evil, as LHC data would be unusable if we did not make these cuts, however any improvements to the efficiency of these cuts allows us to make use of more of our potential data, with no changes to our (expensive) experimental apparatuses. A possible corollary we hope is that by studying the theoretical coherent behavior of WBF is that it may possibly lead to smarter cuts in phase space, as a coherent treatment of the simulated process may show characteristic properties of WBF not prominent in more incoherent representations.

Chapter 3

Event generators

Particle physics is expensive. As an example, during its first run the Large Hadron Collider had running costs of almost 300 million Swiss Francs per year [36]. This creates a problem, as there are many more experiments we would like to run than we can. In particular a way to make predictions for, as well as comparisons against, experimental results would be of imperative value. As such, the need for event generators is naturally created. In particular event generators can be run completely within the Standard Model, as to look for discrepancies between theory and experiment, or they can be modified to simulate BSM physics. The event generators such as PYTHIA [37], HERWIG [38], SHERPA [39] are commonly used in the theoretical and experimental particle physics community for the simulation of these events at particle colliders, and for the case of this research they are used to simulate WBF events to LO+LL accuracy, for which we will be using the PYTHIA event generator.

3.1 Basic Event Structure

The general structure of how event generators calculate collider events can essentially be broken down into three main components. The Hard Process, the Shower Process and Hadronisation; with other intermediate steps also present.

- **The Hard Process**: This is where we calculate the scattering amplitude of our process to fixed order in perturbation theory. This is know as a "hard" process as we can use a factorization Ansatz [40], so long as the process involves a large (hard) momentum transfer $\gg \mathcal{O}(1\,GeV)$. For LO processes event generators typically store the matrix elements for the majority of LO processes (typically at least most $2 \to 2$ and $2 \to 1$ processes, along with other common processes), while NLO processes need to be generated before hand in dedicated matrix element generators such as Powheg-Box [41] and MadGraph5_aMC@NLO [42]. As of 2020, the generation of NNLO has not been fully automated, with these calculations only able to be done on a case by case basis [43].

- **Parton Shower**: The parton shower calculates radiation corrections to the hard process of all orders in perturbation theory to a leading logarithmic (LL) accuracy. This is where we we arrive at the convention of stating our generator to $N^nLO + LL$ accuracy, where the N^nLO is the order of the hard process and LL is the shower on top of the hard process. The parton shower is a necessary process as, by nature of the high momentum transfers, colour charged particles are strongly accelerated

producing QCD radiation. This radiation is eventually seen in the form of objects such as QCD jets, and thus for a full picture of the event these radiative corrections need to be simulated.

- **Multiple Parton Interactions (MPI)**: This takes into account effects due to multiple parton interactions, that is, the fact that multiple partons within a hadron can interact in an event, which are modeled by secondary parton showers [44]. In practical terms MPI can be considered a "noise" term that will smear out effects present in a shower.

- **Matching/Merging**: These (optional) techniques extends the shower treatment with an accurate treatment of extra high p_T jets, with special attention needed to avoid double counting.

- **Hadronisation**: The last step for the event generator is hadronisation. By the principle of colour confinement we know that all out coming particles must be overall colour neutral, leading to hadronisation of left over quarks and gluons produced by the shower process. Since hadronisation occurs in the non perturbative regime of QCD it is currently beyond the scope of our theories to provide a complete description of the process[1]. As such we must use *a posteriori* knowledge, we know that hadronisation *must* occur, since it does, and as such base models around experimental evidence we have gathered about the process as well as general features of QCD. The two main competing models for hadronisation are the string model [45, 46] and the cluster model [47], which use different use different post-perturbative observations to model this behavior.

While fundamentally based on similar techniques, the exact implementation of MC generators can vary between different generators. Even then this does not capture the full picture, as each generator contains their own variants for the shower process (see section 3.2); for example as of version 8.303 PYTHIA contains many fundamentally different parton showers such as: the default shower (known as the simple shower), VINCIA and DIRE (along with a dipole recoil scheme which introduces a fundamentally different shower for IF radiation to the default shower).

In terms of coherence arguably the most interesting and important component of an MC event generator is the shower process. The hard process, by it's nature, captures all of the coherence in a process for a given order. Hadronisation, by contrast, captures coherence as a consequence of the models we use to capture the physics of colour confinement. In contrast as we'll see the treatment of coherence in the shower process is highly dependent on the exact models we choose. As such if one wishes to explore the coherent behavior of Weak Boson Fusion events the key stage to focus on is the shower process, which is what I shall be focusing on for my thesis.

---

[1]Lattice QCD does provide us a method of solving non perturbation QCD, however at this stage the problem of hadronisation has not been solved using this formalism.
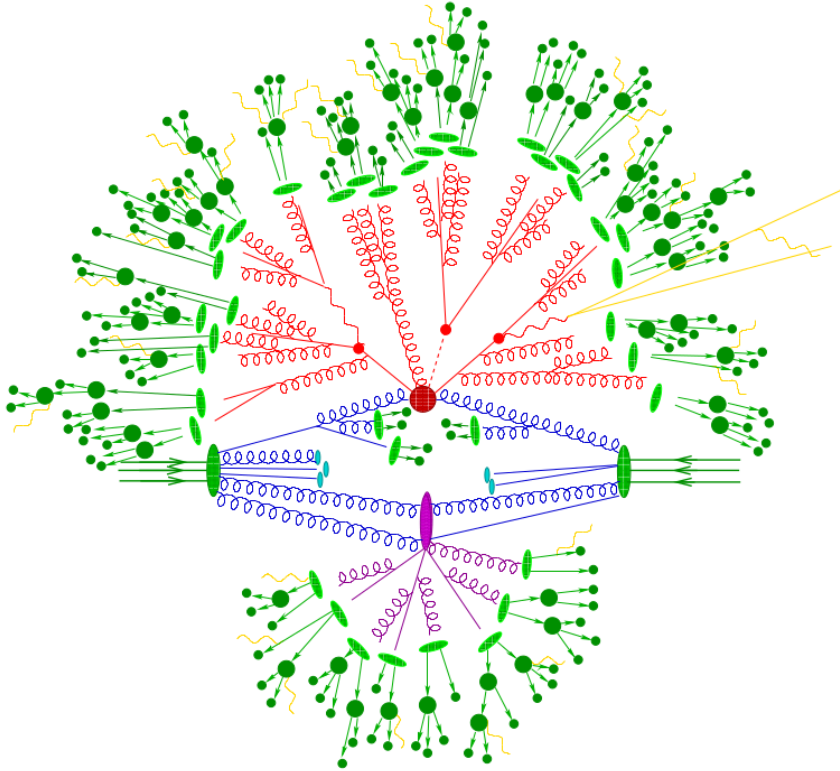
Figure 3.1: Pictorial representation of a hadron-hadron collision as simulated by a Monte Carlo event generator. The red centre is the hard process, the purple blob is a secondary scattering events (such as via MPI). The red, blue and purple lines are the parton shower. The light green and dark green are hadron clustering and hadron decays respectively, while the yellow lines are soft photon radiation. From [39]

3.2 Parton Showers

As discussed previously a parton shower, also called the shower process, calculates the higher-order QCD radiative corrections to the hard process by considering consecutive splittings of 1 particle into 2 particle (or, as we will soon see, the radiation of three particles from a 2 particle colour dipole). The parton shower exists to solve a seemingly simple problem, how can we add radiative corrections to the hard process? That is, how can we add successive gluon emissions to our hard process? The simplest answer would be to calculate our hard process to higher and higher orders, however this approach is not feasible as can been seen in table 3.1 the number of Feynman diagrams required to calculate the QCD radiation corrections quickly becomes insurmountable.

Number of External Gluons	Number of Feynman Diagrams
3	1
4	4
5	25
6	220
7	2485
8	34300
9	559405
10	10525900

Table 3.1: Number of tree-level Feynmann diagrams for the gluon scattering process $gg \to (n-2)gg$ [48]. The number of Feynman diagrams grows faster than $n!$ and it quickly becomes impossible to sum all diagrams. Currently the practical limit for calculating most collision cross sections is NNLO (though some N^3LO results exist, for example N^3LO corrections for Higgs production via WBF [49]), though the process has only been automated to NLO.

Another approach would be to factorize the corrections in terms of the hard process matrix element. What do I mean by this? By this I mean being able to write the born matrix element and the matrix element of the new gluon emission as:

$$|\mathcal{M}_{n+1}|^2 \propto \alpha |\mathcal{M}_n|^2, \tag{3.1}$$

for some splitting factor α. If this can be done then the matrix element corrections can be iterated using a Monte Carlo Markov Chain, capturing the radiative corrections to all orders. It turns out two important limits of this spectrum are factorizeable: the soft and collinear limits, that is, the limits at which gluons are completely soft (when the outgoing gluon has infinitely long wavelength, hence no energy) and the limit at which gluons are fully collinear (where the angle between the gluon and mother particle is 0°). Since radiative corrections are dominated by soft and collinear gluons due to the divergence of these propagators we only need consider these two limits, along with process-dependent non-singular terms, to have a full description of the radiative corrections to the hard process to a leading logarithmic accuracy.
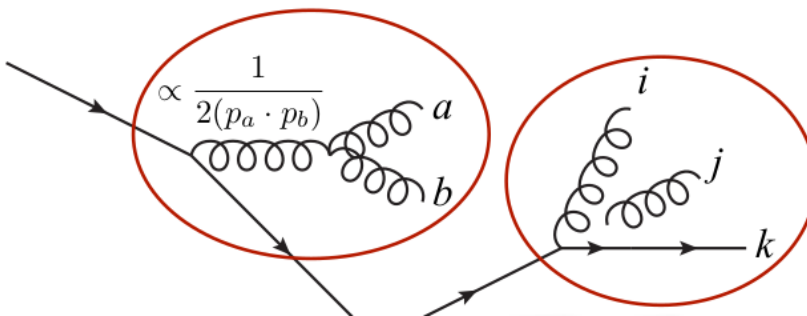
Figure 3.2: Feynman diagrams for the collinear (left) and soft (right) limits for gluon radiation. [10]

In the collinear limit we find that the matrix element squared of the emission of a gluon b from original particle $a + b$ factorizes as:

$$|\mathcal{M}_{n+1}(\ldots, a, b, \ldots)|^2 \rightarrow g_s^2 C \frac{\hat{P}(z)}{2(p_a \cdot p_b)} |\mathcal{M}_n(\ldots, a+b, \ldots)|^2, \tag{3.2}$$

where g_s is the strong coupling factor, C is the colour factor and $\hat{P}(z)$ is the DGLAP[2] splitting kernel, which is the derived from the DGLAP equation and captures the collinear poles as a function of momentum fraction z [50–52].

Similarly the soft limit for a gluon j emitted from (I, K) colour antenna is:

$$|\mathcal{M}_{n+1}(\ldots, i, j, k, \ldots)|^2 \rightarrow g_s^2 C \frac{(p_i \cdot p_k)}{(p_i \cdot p_j)(p_j \cdot p_k)} |\mathcal{M}_n(\ldots, I, K, \ldots)|^2, \tag{3.3}$$

where $\frac{(p_i \cdot p_k)}{(p_i \cdot p_j)(p_j \cdot p_k)}$ is known as the soft eikonal factor, which captures the poles of the soft limit.

The collinear and soft limits for QCD radiation are factorisable, universal - they apply in any context, and are only dependent on the previous state. As such a simple guess would be that it would be possible to apply these gluon splittings, one after another, as a Markov chain defined by some "splitting probability" up to a point where perturbative QCD is no longer valid and we must consider the hadronisation process. This is exactly what happens, with the main difference between methods being whether we only use the collinear limits or whether we include the soft limits as well.

There is one question we have left before moving on, that is what order of perturbation theory are we working in? The answer is all of them; the parton shower captures all fixed orders of perturbation theory, but importantly it captures then up to what's known as the leading logarithm (LL). As such we have an approximation for all orders, but only the hard process is known beyond the LL. This LL shower can be improved by matching/merging, which involves replacing some of the shower process with exact QCD results in perturbation theory. See [53] for more information of this process.

---

[2]Dokshitzer-Gribov-Lipatov-Altarelli-Parisi
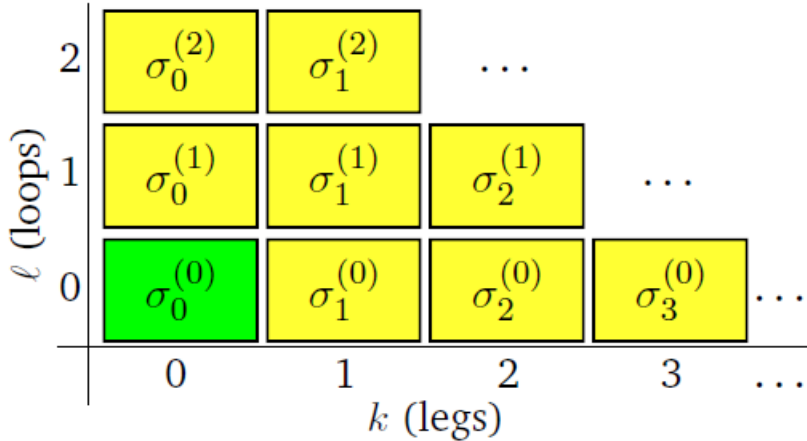
Figure 3.3: Coefficents of the perturbative series with a LO hard process and LL shower process; green represents full perturbative coefficients and yellow represents LL approximations. As can be seen the shower process captures the LL of all orders, while the hard process captures the full coefficients only for a fixed peturbative order [54].

3.2.1 Sudakov factor

At the core of the shower process is the the so called Sudakov factor [55], which characterises the probability for no branching to occur between two "time" scales. It takes the form:

$$\Delta(t_0, t_1) = \exp(-\int_{t_1}^{t_0} dt\, f(t)), \tag{3.4}$$

where t_0 and t_1 are the initial and final "times".

There are a few subtleties when it comes to the Sudakov factor. Firstly the "time": while it can be, and often is intuitively thought of as a time, in practice this is usually calculated in terms of some energy scale $t \sim Q^2$ or $t \sim \ln(Q^2)$, with the Markov chain beginning at Q^2_{Hard} and ending at $Q^2_{\text{Had}} \sim 1\,GeV^2$.

Secondly there is the analytical form of $f(t)$. The form of this function has been intentionally left vague as its form depends highly on the formalism used for the particular event generator. For example PYTHIA by default uses the form:

$$f(t) = \int dz \frac{\alpha_s(t)}{2\pi} \frac{\hat{P}(z)}{t}, \tag{3.5}$$

for transverse momentum-ordered showers [56]; where $\hat{P}(z)$ is the DGLAP splitting kernel.

From here we can simulate the event branching using what is known as the Sudakov algorithm. First we set the Sudakov factor to some random number R_t uniformly generated on $R_t \in [0, 1]$ and solve the equation:

$$R_t = exp(-\int_{t_1}^{t_0} dt\, f(t)), \tag{3.6}$$

for t_1. Here we have t_1 as our time where our gluon branches. From here we apply the algorithm again staring at t_1 until our we reach $t = Q^2_{had}$.

While this equation can be solved, in practice this is cumbersome as $f(t)$ is often a difficult function to integrate. As such the so called Sudakov Veto algorithm is used to calculate the integrals instead. In the sudakov veto algorithm we replace our $f(t)$ by a simpler "trial" function $\hat{f}(t)$ that satisfies $\hat{f}(t) > f(t)$ for all t. The new trial branchings are then accepted with probability:

$$P_{acc}(t) = \frac{f(t)}{\hat{f}(t)}, \tag{3.7}$$

and rejected with probability:

$$P_{rej}(t) = 1 - \frac{f(t)}{\hat{f}(t)}, \tag{3.8}$$

As $\hat{f}(t) > f(t)$ it is guaranteed that $P_{acc} < 1$ and $P_{rej} > 0$, hence probability is conserved. If we accept, done by generating another random number on $R_{acc} \in [0, 1]$ and accepting when $P_{acc} > R_{acc}$, the Sudakov veto algorithm continues on in the same manner as the normal sudakov algorithm. If we reject we assume take that the branching does not occur but still continue on from out new t_0 generated from this simulation.

Using this sudakov factor we can generate our radiation corrections to the hard process by iterating it over a Monte Carlo Markov Chain. For showers based on this collinear limit (DGLAP-based), the radiation generated falls into two main groups, initial state radiation (ISR) and final state radiation (FSR). ISR is the collinear radiation generated by kicked partons before the hard parocess, it results in a spacelike shower which uses a backwards evolution scheme to create a shower. By contrast FSR uses a timelike shower which is forward evolved. Exactly how these two forms of radiation are treated in the limit of the hard process is generator specific, but they both must agree in some way in this limit, and as we'll see this classification of radiation is not appropriate for the soft limit for antenna showers.

3.2.2 Coherence in Parton Showers

An important property of MC event generators is capturing coherence in the shower process. The simplest showers only use the collinear bremßlung limit and hence are based off the DGLAP splitting kernels. DGLAP kernels are incoherent *a priori*, they do not consider a coherent sum of colour partons and therefore can't be expected to reproduce coherent behaviour[3]. Hints as to how this problem could be solved can be seen earlier in this review when discussing the Chudakov effect. There we can see that the coherent emission of photons obeys some angular ordering property, that is, soft photons are suppressed as a function of their opening angle. One could wonder whether this coherent property could be extended to QCD and indeed, an early attempt to reproduce coherent behaviour while still using the DGLAP formalism is known as angular ordering [57] - which takes advantage of the fact that we can veto soft radiation with angular separation, θ_{ij}, from the mother parton greater than between the angular separation between the two parent partons, θ_{ik}. This reproduces the coherent pattern, but azimuthally averaged. There are

---

[3]The DGLAP kernels are actually soft enhanced at $z \to 1$, however this enhancement double counts the soft gluon radiation leading to an excess of soft gluons in the incoherent treatment of parton showers [53]

other incoherent problems with the DGLAP formalism, for example there are ambiguities with recoiler partons. It turns our that the $1 \rightarrow 2$ kinematics of the DGLAP showers does not conserve energy-momentum in the system. This is a problem, and as such we must chose some kind of recoiler parton to conserve energy-momentum. The exact technique used for this is generator specific, but regardless this is an incoherent process. We also have ambiguities with ISR and FSR, as many DGLAP based showers produce these two different forms of radiation separately, meaning that ISR and FSR are incoherent with respect to each over.

3.2.3 Antenna showers

An alternative approach for the shower is instead based off the $2 \rightarrow 3$ kinematics of the soft gluon limit instead. It turns out we can incorporate the collinear limit as well while using these kinematics, the resulting formalism derived from this approach is known as the antenna formalism - with the resulting shower called an antenna shower.

Analogous to the DGLAP splitting kernel, the antenna shower is based on what's known as the antenna function, which can be schematically expressed as:

$$a = \frac{|M_{n+1}|^2}{|M_n|^2},$$ (3.9)

evaluated in the soft and collinear limits, with the exact form depending on whether we are considering initial-initial (II), initial-final (IF) or final-final (FF) radiation. The antenna function can be separated into three parts: the soft eikonal factor, which captures the soft poles; the collinear terms, which capture the collinear poles; and a process dependent finite term, typically denoted by F. Important to note is that this antenna function will reduce to the DGLAP splitting kernel in the strictly collinear limits.

The general form of the Sudakov factor in the antenna shower is thus given by:

$$\Delta(t_1, t_2) = \exp(-\int_{t_1}^{t_2} d\Phi_{\text{ant}} 4\pi\alpha_s \mathcal{C}\bar{a}),$$ (3.10)

where $\mathcal{C}$ is the colour factor of the given $n \rightarrow n+1$ branching process and $\bar{a}$ is called the colour-stripped antenna function - the antenna function without colour or coupling factors. The sudakov factor is evaluated in a similar manner to that of DGLAP based parton showers, though we are required to evaluate the antenna phase space, $d\Phi_{ant}$. This phase space factorises, and has a different form depending on whether we are considering II, IF or FF radiation.

Like in DGLAP based shower antenna showers break down radiation into three groups, initial-initial, initial-final and final-final, all of which have slightly different conventions to how they treat the antenna function. The type of radiation depends on whether the colour antenna in question spans two initial state partons, two final state partons or an initial and a final state parton. While II and FF can generally be modeled by ISR and FSR in DGLAP showers IF is a challenge, as it embodies elements of both ISR and FSR. It becomes more clear now exactly why the ISR/FSR separation in collinear showers was a source of incoherence, as that formalism can not coherently model IF radiation. For processes such as WBF where IF radiation is the dominant form this can lead to large discrepancies between different showers when modeling the coherent radiation pattern.

Furthermore unlike using angular ordering with a DGLAP shower this formalism is inherently coherent, with coherence being derived point by point in phase space as opposed

to azimuthally averaged. There is also the advantage that by using $2 \to 3$ kinematics all partons in the antenna shower can be on-shell, while DGLAP based showers are not and require other methods to compute partons as on-shell. As such another source of incoherence in conventional showers is rectified in antenna showers.

3.2.4 Specific showers: Coherence in PYTHIA and VINCIA

Before continuing on to the results of my analysis let's consider some of the specific differences in how PYTHIA and VINCIA simulate coherence in their showers.

To start VINCIA uses the antennae formalism to simulate coherent radiation. As such we expect it to reproduce a coherent radiation pattern. PYTHIA by contrast is a DGLAP based shower and reproduces coherent behavior using other methods. Interestingly PYTHIA does not use angular ordering to generate coherence, instead uses an interesting technique by generating incoherent radiation in the rest frame of a radiating parton dipole, which is then Lorentz boosted to the lab frame which simulates the coherence. As such we get back coherent radiation using a kinematic model, as well as cutting off hard radiation with transverse momentum greater than that of the radiating dipole. This works well for FF radiation, as well as II radiation (which since the partons are located 180 degree from each over coherence is not a large factor in II radiation) however this formalism breaks down for IF radiation. As discussed in 3.2.2 this IF radiation will have to be incoherently separated into ISR and FSR, which will inarticulately simulate the coherence for IF radiation. For processes where IR radiation is not prominent this is a good approximation, however for a process such as WBF as we can see in figure 3.4 where IR radiation is the dominant form produced we would expect PYTHIA to not correctly simulate the coherent radiation pattern.
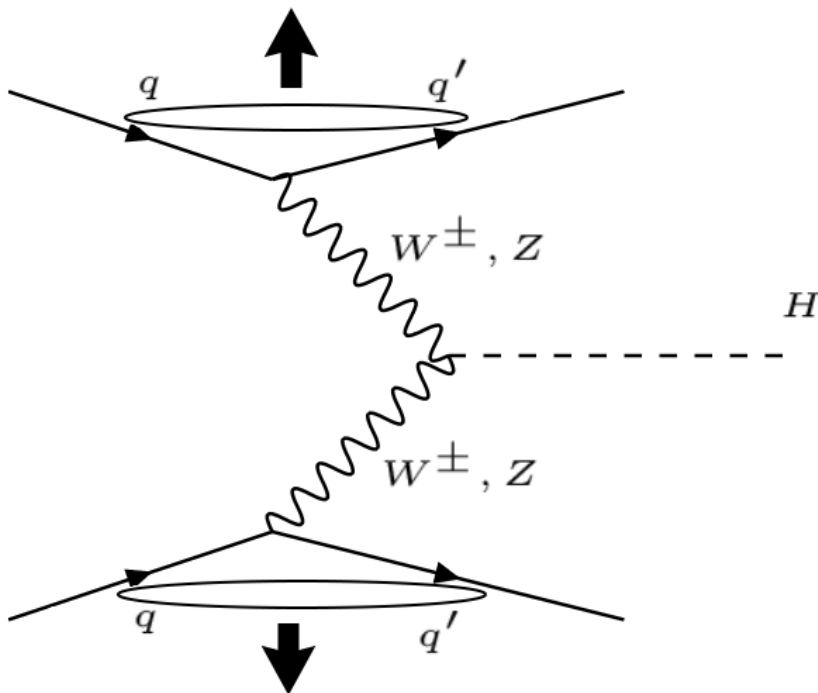
Figure 3.4: Radiation pattern for WBF at LO. The two ovals represent the colour dipoles formed by the initial and final scattered quarks while the arrows represent the IR radiation generated. As can be seen the LO process is dominated by IR radiation.

Chapter 4

Observables, event parameters and Cuts

Before discussing the Monte Carlo results some time should be taken to discuss both some of the common observables used throughout the analysis, the parameters used for the events (particularly for the sake of reproducibility) and the exact WBF cuts implemented in the event analysis.

4.1   Observables

While by no means an exhaustive list, some common observables used throughout this analysis include:

- **Rapidity** (y): Rapidity is a Lorentz invariant measure of relative velocity related to the hyperbolic angle between two inertial frames of reference. Unlike conventional measures of relative velocity in special relativity rapidity is additive, hence calculations using this obversable are made significantly simpler. Typically in collider physics we are only intereseted in the rapidity relative to the beam axis (z direction), which can be written in terms of a particles energy and momentum as:

$$y = \frac{1}{2} \ln \left(\frac{E + p_z}{\sqrt{m^2 + p_T^2}} \right), \tag{4.1}$$

  which is Lorentz invariant in the z direction.

- **Pseudorapidity** (η): This is a measure of the longitudinal angle θ, given by:

$$\eta = -\ln(\tan(\frac{\theta}{2})). \tag{4.2}$$

  Pseudorapidity and rapidity are equivalent for massless particles, and approximately the same when $m \ll |\mathbf{p}|$, which is often a good approximation in collider contexts. Since particle production is roughly a constant as a function of rapidity, pseudorapidity is a more logical choice for measuring the angular distribution of outcoming particles compared to using the longitudinal angle θ; furthermore pseudorapidity only depends on θ while rapidity requires knowing a particles energy, making it a far easier measure to use in practice. High values of $|\eta|$ are close to the beam axis and are often referred to as "forward".

- **Transverse momentum** (p_T): Transverse momentum is simply the x and y components of momentum i.e. $p_T^2 = p_x^2 + p_y^2$. In each event at a collider a significant amount of the beam energy, which is along the z direction, is lost down the beam pipe [58]. As such the net z component of momentum can not be constrained, while the while the x and y components are known to be have net zero momentum each. As such it becomes much simpler to only consider the contributions from the x and y components of momentum.

- **Scalar sum of transverse momentum** (H_T): H_T (sometimes referred to as $\sum |p_T|$) is simply the scalar sum of the transverse momentum of particles withing a given region, which can be modified to only include charged particles with small pseudorapidities (to simulate the tracking limitations at the ATLAS/CMS detectors). This is a reasonable measure of the activity of particles in a given region as it will always increase when there are more particles present, unlike the vector sum which may not. Furthermore this quantity can be used as the p_T of a jet (though we do not cluster our jets using this method in this thesis) and as such it is a useful observable to compare to in Monte Carlo studies, particularly if one is interested in soft behavior over an arbitrary region.
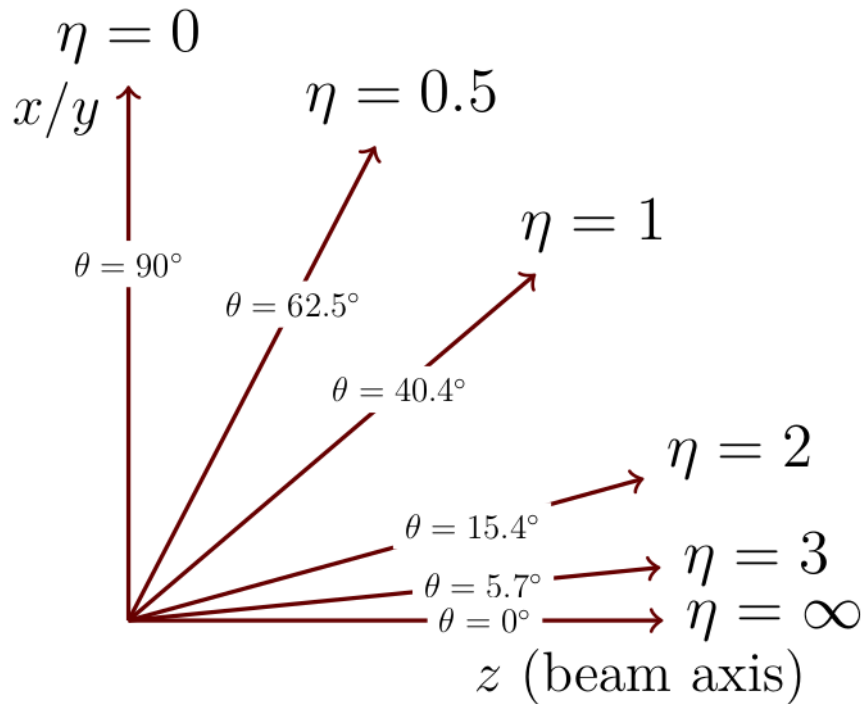
Figure 4.1: The relationship between pseudorapidity and longitudinal angle θ. Differences in rapidity close to 90 degrees of the beam axis are exaggerated, while high values of η correspond to angles close to the beam axis.

4.2   WBF cuts and event parameters:

For the analysis conducted here we have used the following jet definitions/cuts: For all jets we have that:

- $p_T > 20$ GeV

- Jet radius $R = 0.4$, where the jet radius is defined as $R^2 = y^2 + \phi^2$

- Only consider the region $|\eta| < 5$ - based on the detector range of the ATLAS and CMS detectors at the LHC

- Jets clustered using FASTJET analysis package [59] with anti-k_t algorithm [60]

- Jets do not cluster Higgs decay products

For the two tagging jets (j_1, j_2):

- $m_{j_1, j_2} > 600$ GeV

- $|\Delta \eta_{j_1, j_2}| > 4$

- $\eta_{j_1} \cdot \eta_{j_2} < 0$

These simply ensure that the jets are sufficiently hard, have a large separation in pseudo-rapidity and are located in opposite hemispheres.

Finally we have the third jet (j_3) veto. Here we veto events containing jets that are located within the pseudorapidity between the two tagging jets. This third jet veto comes from the expected coherent suppression between the two tagging jets. Of course this is merely an experimental cut. We can, and do, generate actual WBF events containing these third jets and since they are particularly sensitive to coherence we will be studying this third jet. However unless otherwise specified we will be implementing the third jet veto to all other events where the third jet is not the focus of the analysis.

Lastly for my analysis unless otherwise specified we will be using the default settings for PYTHIA/VINCIA with the following exceptions:

- **Only considering the Higgs$\rightarrow \gamma\gamma$ decay channel**: What the Higgs specifically decays into is not of interest to us, as the coherent behavior of weak boson fusion is not dictated by the Higgs decay products. As such the only consideration for what Higgs decay channel to use is simply by what is the simplest to implement/analysis; which since the photon decay channel is the cleanest decay channel (no QCD jets from decay products, only two easily identifiable hard photons to detect) this is the natural choice for this analysis

- **Hard photons do not branch**: The photons generated from the hard process have a chance to split into $l\bar{l}$ pairs. Once again since we are only interested in the coherent behavior we simplify our analysis by only considering events where the two photons from our LO event do not decay.

- **Multiple parton interactions (MPI) and Hadronisation off**: MPI in practice defines other shower processes that occur due to scatting off multiple partons. These showers occour at lower scales and hence in practice mannifest as "noise" on top of the base results from the shower process. Hadronisation, by contrast, is fully coherent; it can thought of as the non-perturbative dual of the colour dipoles we see in perturbative QCD[1]. Since hadronisation occours at might lower scales then the

---

[1]To be more precise it is the hadron strings, from the string model, are the non-perturbative dual of perturbative colour dipoles. Of course there is the cluster model, a competing hadronisation model, however it is typically believed that the string model is the more "physical" model of hadronisation; though these discussions of hadronisation model and their merits are well beyond the scope of this thesis.

hard process starts at we can't expect it to be able to create new jets per se, but some shifting behavior due to hadronisation can be expected. Regardless, MPI and hadronisatio both obscure effects we wish to see at the parton shower level, and as such for the majority of this analysis are switched off.

- **Run at 1,000,000 events with** $\hat{s} = 13$ **TeV**: All runs will be calculated with 1,000,000 events, with error bands quantifying the statistical uncertainty of the histograms presented. To simulate events at the LHC we will use a centre-of-mass energy of 13 TeV.

Chapter 5

Weak Boson fusion event generation

In this section I present the results from running the WBF analysis using the PYTHIA and VINCIA showers. Each section focuses around a different parameter we wish to observe, beginning with analysis of observables we predicts to be sensitive to coherence within the WBF analysis and ending with a preliminary analysis of other extensions to the main analysis such as hadronisation and factorisation effects. All histograms are presented with error-bands which represent the statistical fluctuation of values within the histogram bins.

5.1 Third Jet Transverse Momentum

As discussed earlier coherence in weak boson fusion manifests itself in the form of coherent suppression of radiation in regions of small rapidity/pseudorapidity and small p_T for WBF. As such if we believe there are noticeable differences between how PYTHIA and VINCIA are simulating coherence in WBF then it is this region of phase space that we should bring our attention to. Given this a good observable to focus on is the third jet j_3. The third jet should be very sensitive to coherence as it is located purely within this small pseudorapidity region of phase space, as such the third jet makes a good candidate for an observable in the context of coherent analysis of WBF.

A reasonable unit to plot the third jet against is transverse momentum. Since we expect QCD radiation to be suppressed between the two tagging jets we would expect if VINCIA reproduces coherence more accurately than PYTHIA then transverse momentum spectrum of the third jet should be suppressed. In particular we should expect that PYTHIA produces more soft (low-p_T) jets, as the coherent suppression is also a function of transverse momentum.
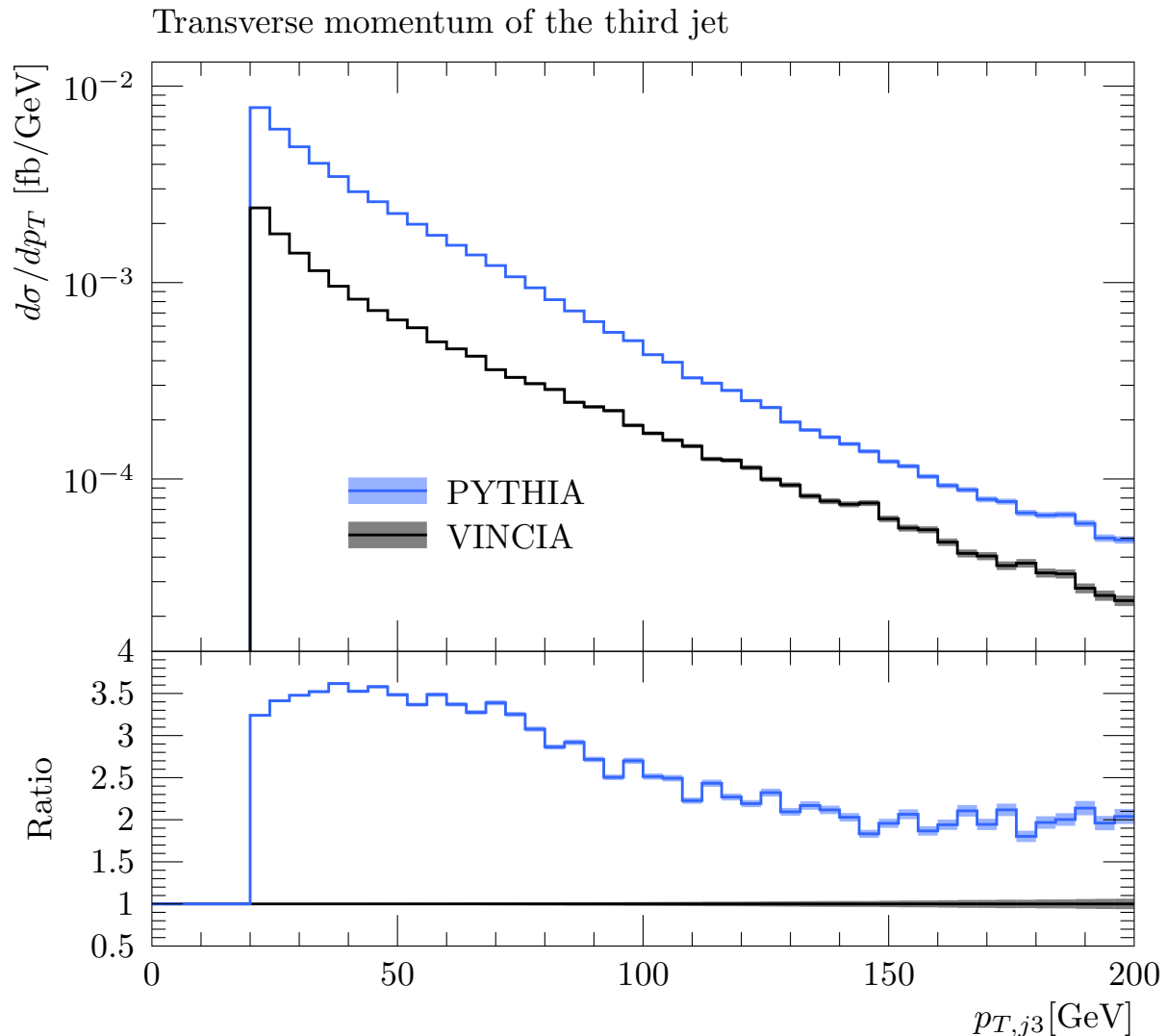
Figure 5.1: Transverse momentum of the third jet for PYTHIA and VINCIA. PYTHIA produces third jets a factor of up to 3.5 times more than VINCIA does. This difference appears to decrease as a function of p_T.

Looking at figure 5.1 we can see that this assumption of a coherent difference in the third jet holds true. Here we see a factor 2-3 difference in the rate of third jets produced by PYTHIA and VINCIA. As we know by nature the antenna functions used in VINCIA are coherent from the ground up, and as such we can interpret this histogram as PYTHIA placing more radiation in this third jet region of phase space, which leads to a nonphysical inflation of the number of third jets present. The trend seems to also correlate with the third jets transverse momentum, with low p_T jets seeming to be more over-represented in PYTHIA while high p_T jets being described with a smaller disagreement - though this argument is best saved for the following section where it is shown more conclusively. Even so, relatively hard jets of $p_T \approx 200$ GeV are still over-represented by a factor of 2. These differences alone already are cause for doubt on the ability of DGLAP based showers to accurately describe the coherence radiative physics of processes such as WBF which heavily depend on an accurate description of IF QCD radiation.

5.2 Third jet pseudorapidity

Another unit we can compare the third-jet observable to is pseudorapidity. We know that the coherent suppression of radiation in WBF is enhanced for low values of $|\eta|$, as such if PYTHIA is not reproducing the coherent radiation pattern we would expect it to break down for low values of η. Furthermore if we want to show that this should be more pronounced for low p_T jets we can split up our distributions depending on their transverse momentum. Only plotting the pseudorapidity distributions of third jets over a range of 25 ± 5 GeV, 50 ± 5 GeV and 80 ± 5 GeV to see how these distributions vary.
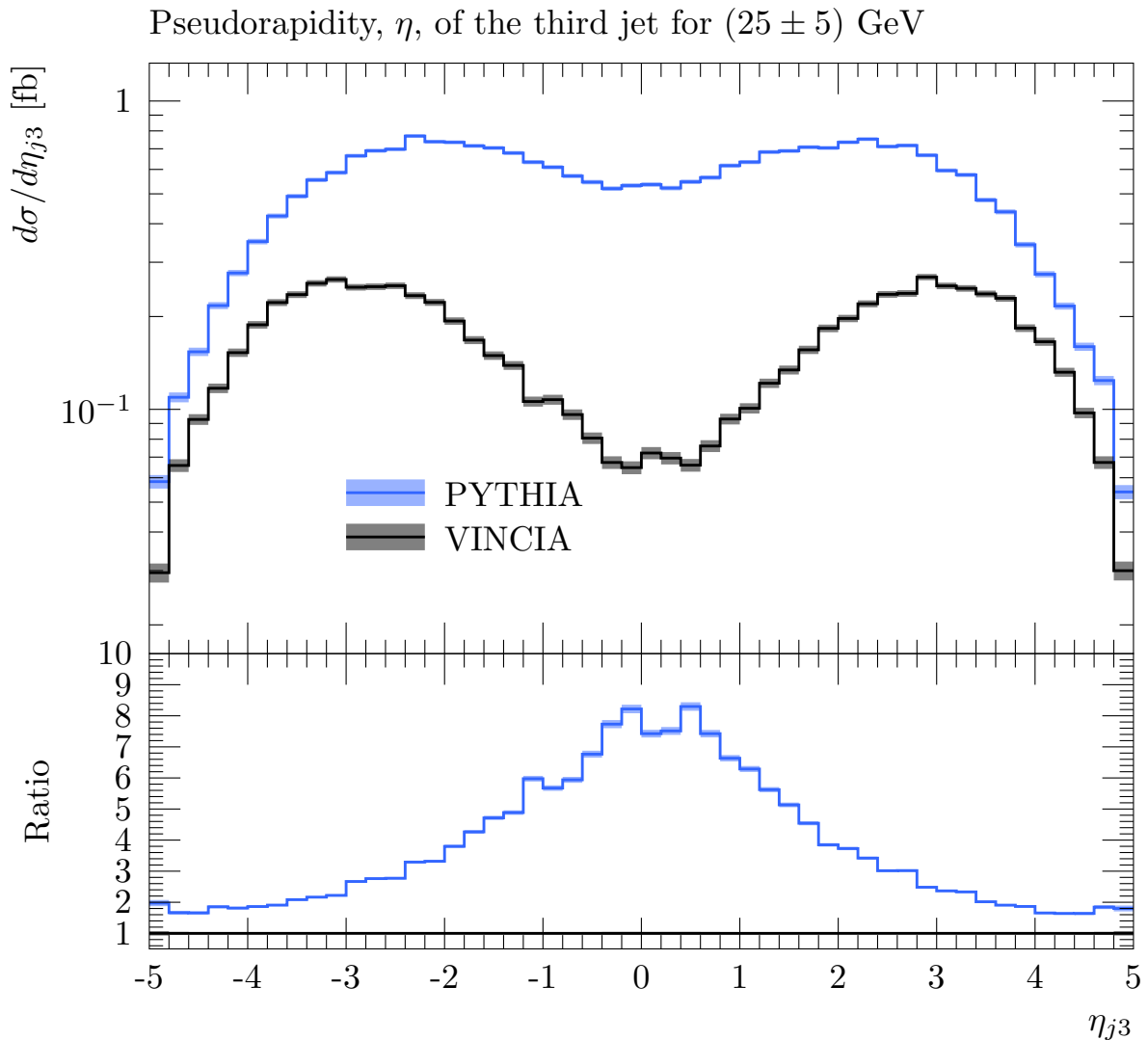
Figure 5.2: Pseudorapidity of the third jet values in the range of $p_T, j_3 \in [20, 30]$ GeV

Looking at the distribution for low p_T jets centered on 25 GeV in figure 5.3 we can see a **large** difference between the number of jets PYTHIA and VINCIA predict for this small pseudorapidity region. Around $\eta = 0$ we reach a factor of 8 difference between these two models, this difference diminishing to a factor 2 close to the edge of the calorimeter region ($|\eta| \approx 5$) at the ATLAS/CMS detectors. Once again we arrive at the same conclusions we had previously, that the coherent suppression for small pseudorapidities is not being captured in PYTHIA when compared to VINCIA, in essence PYTHIA is placing more low-p_T particles in this region then there should be.

As alluded to before, we expect the coherence effects to be dampened for higher p_T, and as such we would expect PYTHIA and VINCIA to begin to converge for higher transverse momentum.
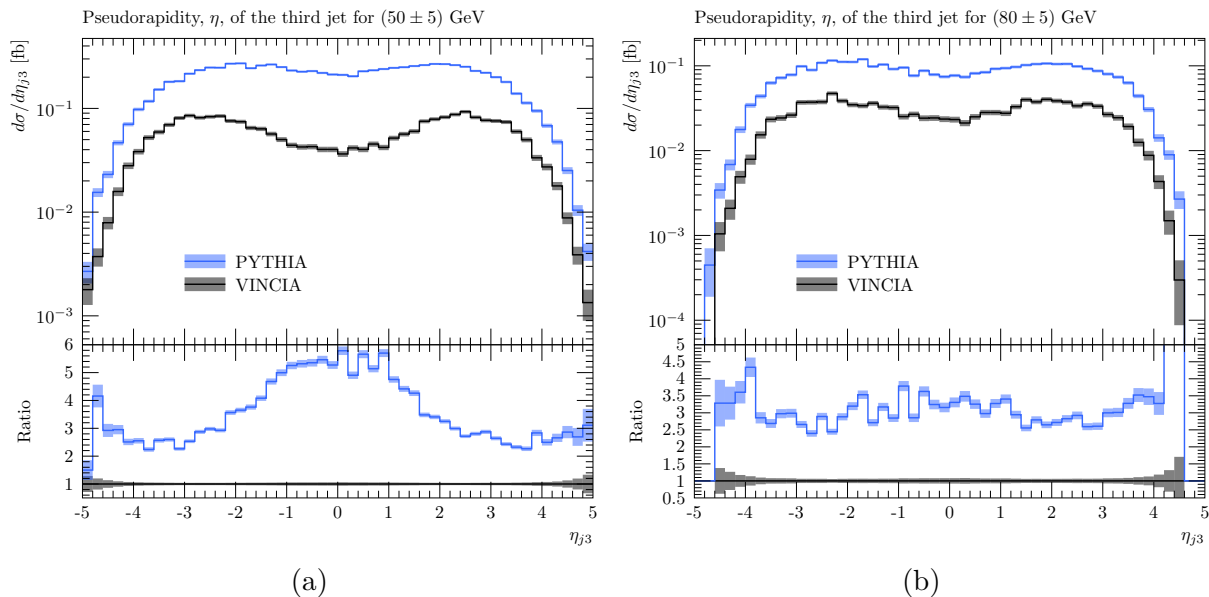
Figure 5.3: (Left) Pseudorapidity of the third jet values in the range of $p_T, j_3 \in [45, 55]$ GeV. (Right) Pseudorapidity of the third jet values in the range of $p_T, j_3 \in [75, 85]$ GeV

Looking at 5.3 this certainly appears to be the case. As we consider larger values for the transverse momentum of the third jet appear to converge for higher values of p_T. By the time we reach a transverse momentum of 80 GeV coherence in pseudorapidity appears to vanish, while we still are left with some coherence with respect to transverse momentum, leading to a uniform factor of 3 increase of jets in PYTHIA compared to VINCIA.

These plots, along with that of the third jet p_T spectrum evince that coherence suppression of the third jet that simply is not captured in PYTHIA. This is of particular concern not just to the theoretical community but also to the experimental, as if one were to implement the third jet veto in PYTHIA as opposed to VINCIA, due to the over-representation of third jets in PYTHIA we would be left with a smaller proportion of useful data that survives the third jet veto.

5.3 H_T in regions of pseudorapidity

Another observable to consider is the scalar p_T sum, H_T. It can be used as an indicator of the amount of jet activity in a given region - as unlike the vectorial sum of p_T, H_T always increases when we have more particles in a given area. A good region to check coherent suppression would be the region between the two tagging jets, specifically around the midpoint between the tagging jets. We know from studying the third jet that this region is where the bulk of coherent suppression in phase space is occurring, as such we would once again expect suppression for low p_T, and hence low H_T. Given the range of the charged particle trackers at the ATLAS detectors are $|\eta| < 2.5$ we also limit ourselves to charged particles within this region.
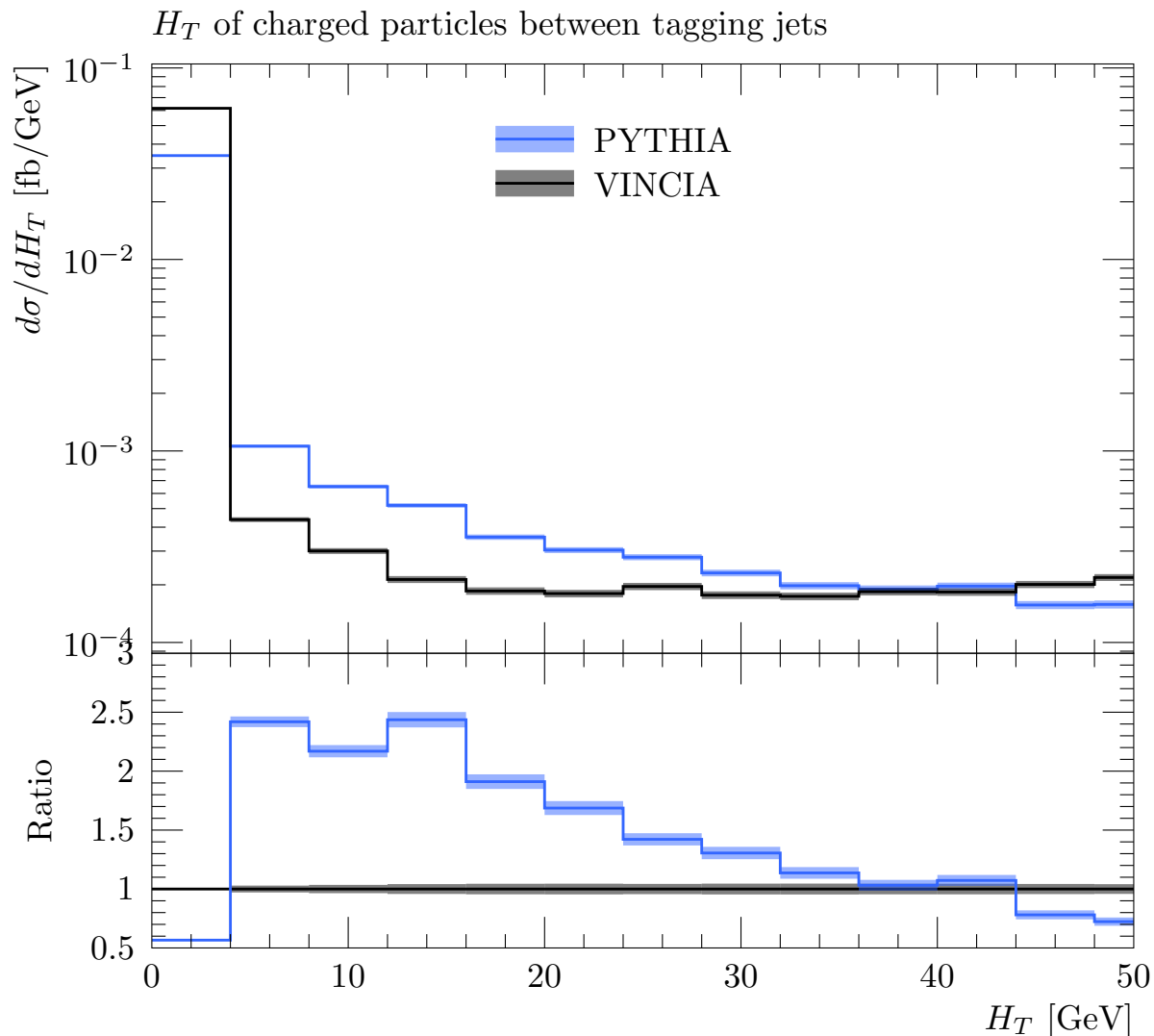
Figure 5.4: H_T of charged particles in the region $\eta \pm 0.5$ around the midpoint of the tagging jets. This region can not be larger than $|\eta| = 2.5$, which simulates the experimental limits of the ATLAS and CMS detectors.

Figure 5.4 tells a similar story to what we found in section 5.2, PYTHIA appears to be producing low p_T radiation in abundance in this region, while VINCIA is saying that this excess radiation in nonphysical. Around 45 GeV this swaps around and PYTHIA produces less high p_T radiation than VINCIA, and simillarly we have another cross-over point at the end on the first bin in our histogram. In terms of how to think about what is occurring at the first bin: in the beginning both PYTHIA and VINCIA start with the same amount of events (as both generators are run 1M times) all in the 0 bin. As events are simulated the generators pluck the data from this zero bin out towards whichever bin the simulation predicts it should go, as such there must always be some cross over point between our two generators if we want to preserve the number of events produced in our histograms. The other cross-over point is also interesting; the fact that this other point occurs as early as it does in p_T demonstrates how strongly the suppression is correlated with soft radiation, as opposed to hard radiation.
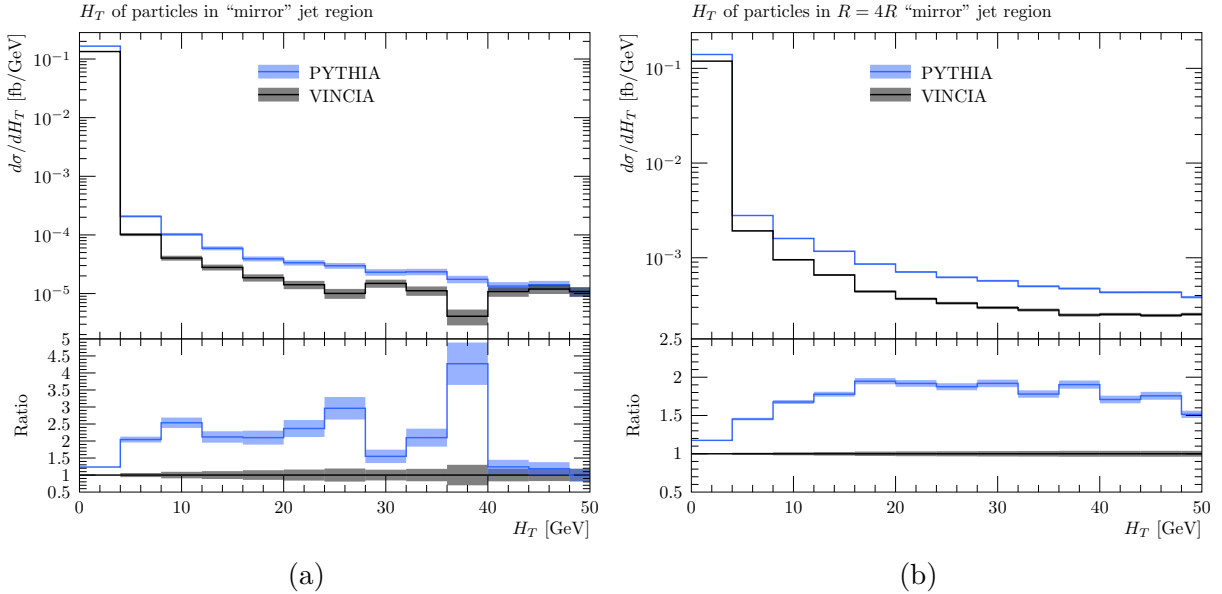
Figure 5.5: (Left) H_T of particles in the "mirror" jet region (Right) H_T of particles the "mirror" jet region, this time with a larger jet radius 4 times the original

Another interesting region to test the H_T observable on is the "mirror" jet region. This is the region directly mirrored in pseudorapidity and azimuthal angle to the tagging jets. Given that these are completely opposite the two tagging jets, which contain the bulk of QCD radiation in this process, we would once again expect coherent suppression in this region. As we will see the amount of radiation in this region of phase space is so small that the statistical uncertainties become large even for 1M events, as such a reasonable solution is to also consider a larger region of phase space with a radius 4 times larger than the original jets. This will include more radiation, and as a result contain more statistically significant results, however will contain radiation that is less susceptible to coherence; possibly making the effects of coherence less pronounced in our histograms. As such a good compromise to to consider the behavior of both scenarios, and compare their effects together.

As seen in figure 5.5 these coherent effects appear to mirror what we found for the H_T sum in the region between the tagging jets. We see significant suppression of H_T in VINCIA that is not reproduced in PYTHIA. Furthermore these effects appear to continue on beyond the original jet radius, with significant differences in H_T appearing event at the $4R$ radius mark. Interestingly the coherence in the mirror jet region appears to not be as dependent on p_T compared to suppression of radiation between the tagging jets. As can be seen for $H_T < 10$ GeV PYTHIA and VINCIA appear to agree more than for harder radiation, which is an effect not seen in figure 5.4.

5.4 PYTHIA Dipole recoil

One interesting setting that is worth considering for the PYTHIA simple shower is the dipole recoil setting [61]. At first glance the dipole recoil setting changes how PYTHIA treated the recoiler parton needed for energy-momentum conservation which by default uses a global recoil scheme instead. If this was all it did the dipole recoil setting would not be particularly interesting with respect to coherence, however this setting some something

rather interesting - it treats IF radiation (typically split into incoherent ISR and FSR parts) with an antenna/dipole like formalism. As such, we would expect that WBF, dominated by this form of coherent radiation, would match well with PYTHIA with the Dipole setting. Let's test this by considering the third jet p_T spectrum again along with the H_T between the tagging jets.
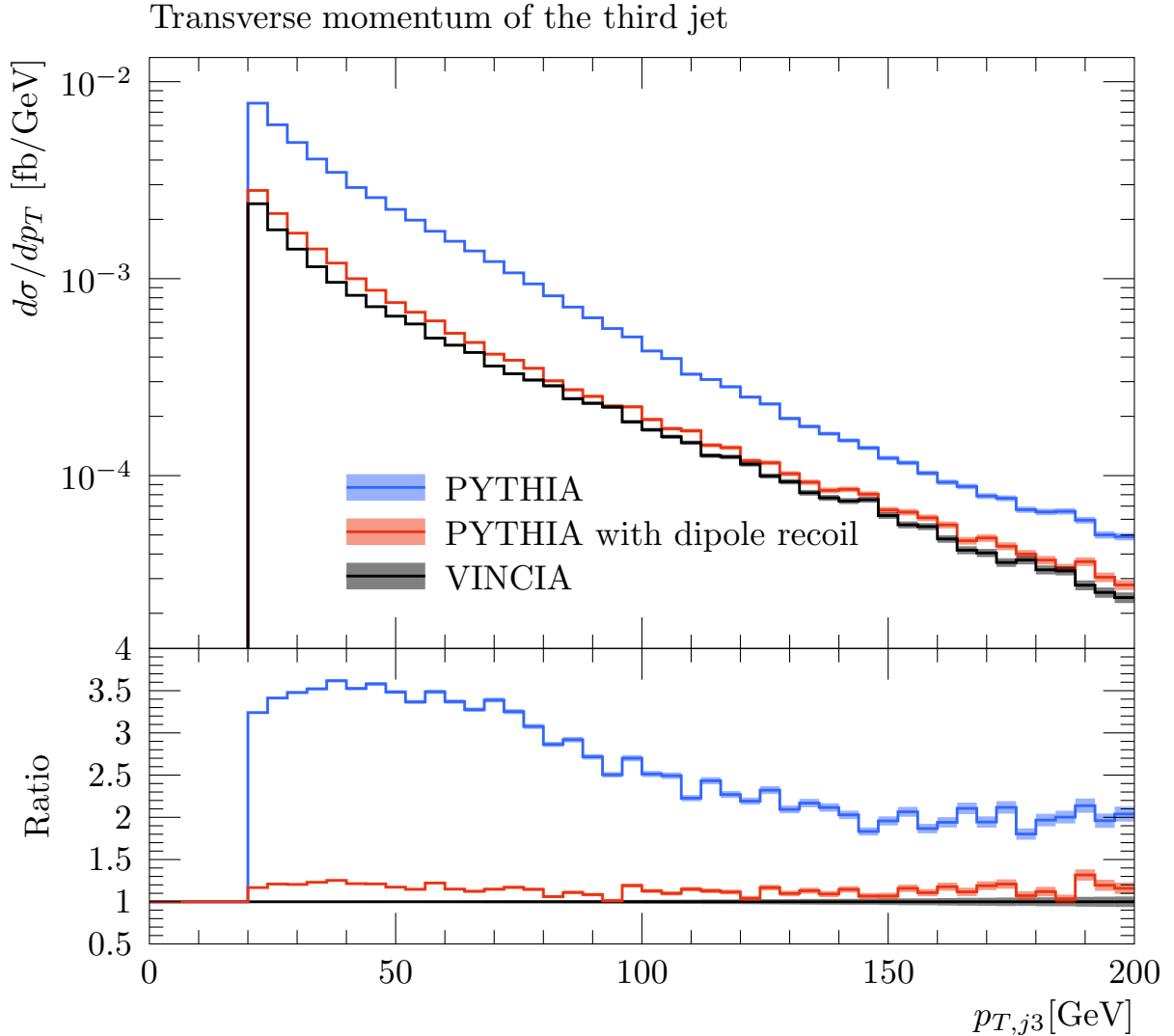
Figure 5.6: Transverse momentum of the third jet for PYTHIA, PYTHIA with dipole recoil on and VINCIA. PYTHIA produces third jets a factor of up to 3.5 times more than VINCIA does, however by turning on the dipole recoil the differences between the two models vanish, with PYTHIA now reproducing the correct spectrum for IF radiation.

As we can see with the correct treatment of IF radiation PYTHIA and VINCIA now agree. Let's also check the H_T histogram to see if these results are consistent.
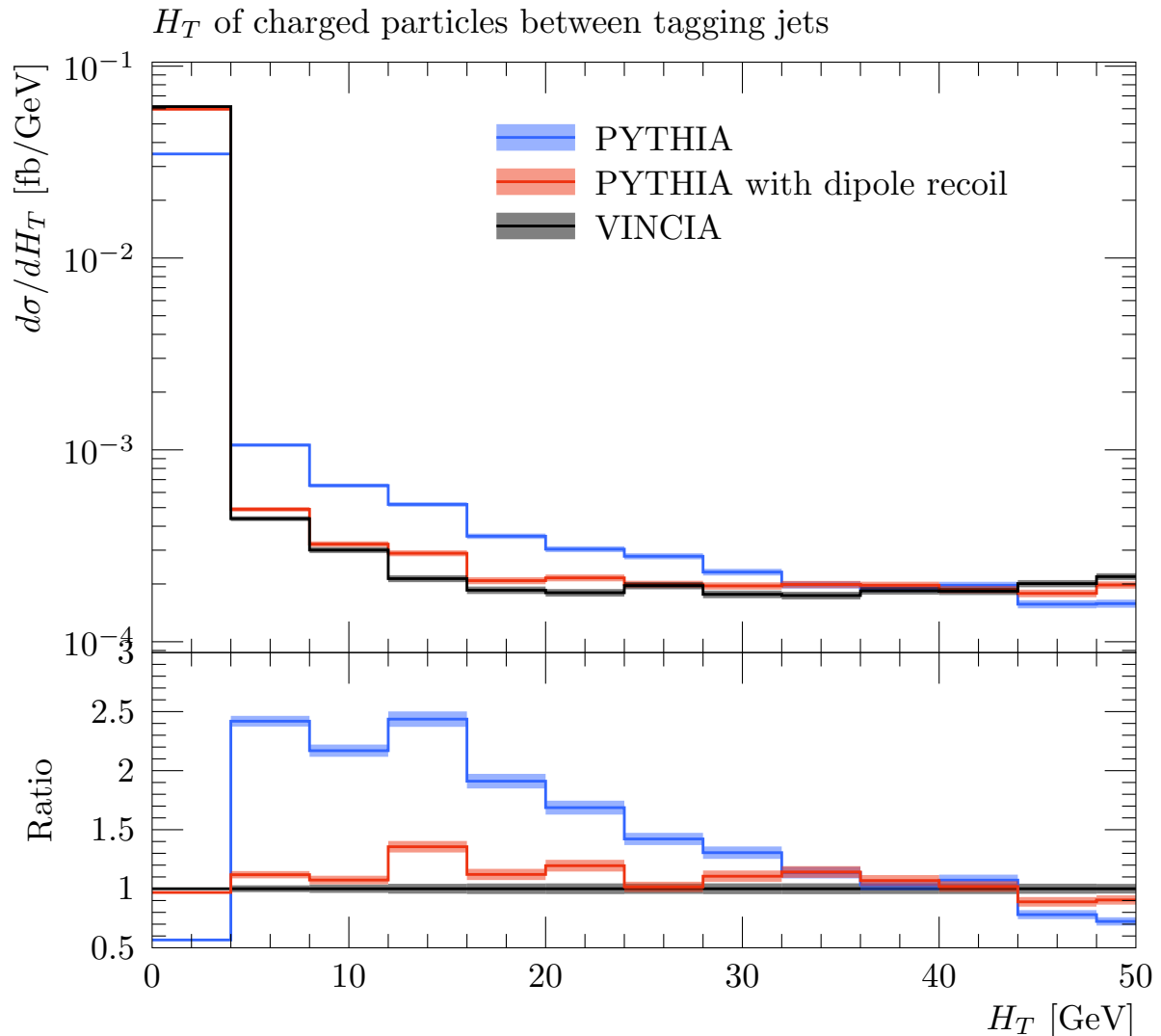
Figure 5.7: H_T of charged particles between the tagging jets. Once again differences between PYTHIA and VINCIA vanish between with the dipole recoil turned on.

Figure 5.7 we can see that this convergence is not a one off - with an antenna treatment for IF radiation the differences between PYTHIA and VINCIA do converge. It is important to note that this required the use of, at the very least, an antenna-like formalism to solve, and as such gives us further indication that the inherently coherence formalism of the antenna shower appears to be needed to capture the coherent physics for WBF.

5.5   Factorisation Scale

While not an effect of coherence per se the differences we see between PYTHIA and VIN-CIA when considering different factorization scales deserves mention. The factorisation scale of a process can be thought of as a measure of the characteristic wavelength λ of the process. For proton-proton collisions this can be thought of as parameterising the scale at which we are probing the proton itself. The structure of a proton is parameterised by what's known as a Parton Distribution Functions (PDF), which at Leading Order (LO) can be thought of as functions that parametrise the probability density of partons within a proton. These PDF's are a function of the facorisation scale, which mimics the behavior

we obverse in proton collisions: at low energies the proton appears to consist of a few "valence-like" partons, and at larger energies the proton appears to be made up of a large amount of constituent elements - quarks and gluons.

This scale is closely related to another important scale we use, namely the shower starting scale. This is the scale at which we begin our Sudakov algorithm, and while the choice for this scale is also arbitrary, typically it is chosen to match the factorisation scale. As such variations of the factorisation scale not only change how the hard process is determined but also the shower process, and as such is of interest to us while studying properties of the shower process in WBF.

There is no "one correct" factorisation scale for a given process, and its choice is somewhat arbitrary. For a t-channel (scattering) processes a reasonable guess is the transverse momentum transfer of the process. For massless particles this captures well the scale at which we are probing the protons, however WBF involves the transfer of rather massive $Z^0/W^\pm$ bosons with masses of approximately 91 GeV and 80 GeV respectively, as such for weak boson fusion the boson masses exchanged also need to be taken into consideration.

This leads us to the factorisation scale PYTHIA uses by default, which is the "geometric mean of the two propagator virtuality estimates"; or in other words the geometric mean of the transverse momenta of the scattered quark with the mass of the transferred weak boson[1]. We can also consider two other choices for factoirsation scales, both of which are larger than our original choice. One possible route is to also consider the generated Higgs transverse mass in the factorisaiton scale, which gives us the geometric mean as above but including the Higgs transvese mass. The second, even larger, option is to use the centre-of-mass energy, $\hat{s}$ of the process. This is the largest factorisation scale that would still be considered somewhat sensible. With all of this in mind considering how factorisaion scale variations would change the showers in both PYTHIA and Vinca is of possible interest, since both showers are built in different ways this may lead to a difference in how the factorisation scale variance presents itself, which in turn may indicate which shower model is more physical with respect to WBF. Let's consider these factorisation scale variations for the pseudorapidity of the tagging jets, which should not show much variation between the two showers.

---

[1]PYTHIA documentation represents this by the transverse mass, $m_T^2 = m^2 + p_T^2$ for the scattered quarks, but replaces the quark mass with the mass of the weak boson. This substitution is written as $m_{TV_i}^2$ for the ith quark.
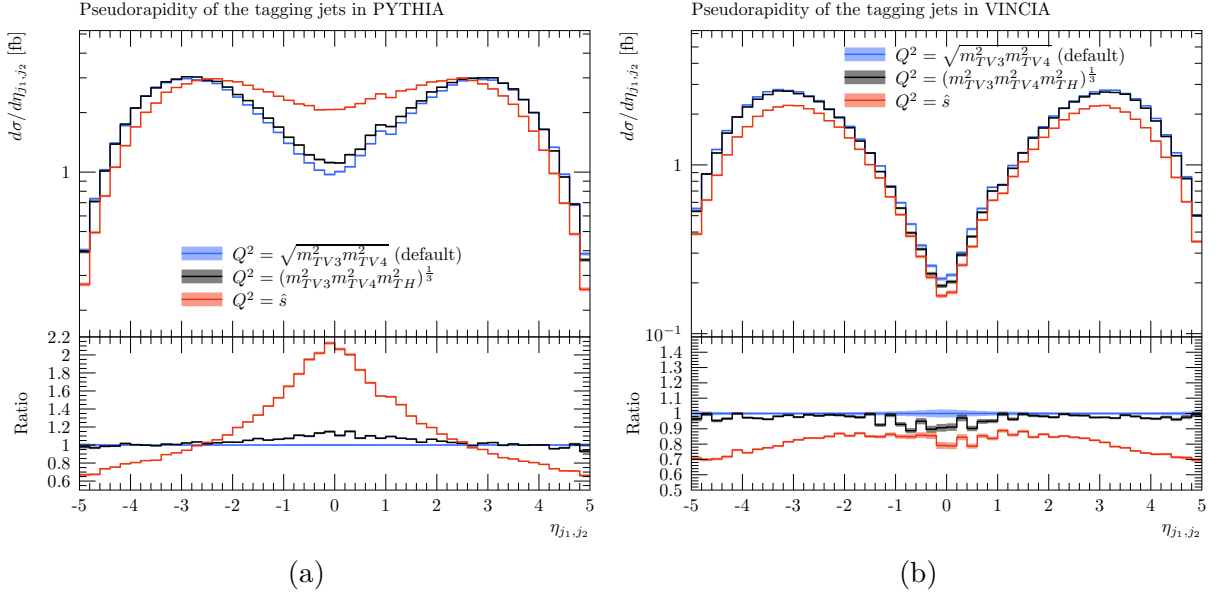
Figure 5.8: (Left) Factorisaion scale effects for PYTHIA, with three variations: the default scale, default scale with higgs transverse mass and $\hat{s}$. (Right) Same, for VINCIA.

As we can see, the factorisation scale affects PYTHIA significantly, with the largest $\hat{s}$ scale producing tagging jets a factor of two times greater in the region around $\eta = 0$. Meanwhile VINCIA is not nearly as affected, the behavior around $\eta = 0$ is almost identical to that of the default factorisation scale choice. This can be explained by considering what is occurring in terms of the colour dipoles present in the shower. Physically the invariant mass (or, for an IF dipole the momentum transfer between the initial and final parton) of a colour dipole system can be considered to be an upper limit of the hardness of radiation being produced by the colour dipole; we can not produce radiation of a higher energy than this invariant mass of our system. VINCIA knows about colour dipoles, this sets an upper bound on the radiation is can produce, limiting us to a smaller phase space available which it will not access even if the factorisation scale is increase. PYTHIA meanwhile does not know anything about these colour dipoles, and as such has access to a much larger (and un-physical) phase space which will generate radiation above the mass of these colour dipoles. This hints to us that VINCIA is reproducing the physics more accurately for WBF, while PYTHIA is not. Varying factorisation scale parameters from the norm breaks some of the techniques PYTHIA uses to mimic coherence, while VINCIA is left relatively unchanged.

5.6 Preliminary MPI and Hadronisation effects

So far in our studies we have only considered the coherent effects from the shower process. This has been done by turning off MPI and Hadronisation in our analysis, so that the effects of the shower process are not obscured by any "noise" or other unwanted effects from these two processes. This does, however, leave us with the question as to whether these effects can still be seen with MPI and Hadronisation on? This is interesting to consider, particularly from an experimental perspective - as if these coherence effects are not visible with MPI and Hadronisation on the differences between PYTHIA and VINCIA would be considered trivial in this context.

As discussed previously MPI and Hadronisation will affect our analysis in different ways. MPI adds "noise" to our spectrum which can wash-out our signal, while Hadronisation is inherently coherent by design, and can add small coherent corrections to our distributions. Nevertheless, we do not expect significant changes to our distributions - we expect to obtain histograms with much more "noise" due to MPI in particular.

To see the impact of these settings turned on for WBF coherence, we should look at distributions where coherence effects are most prominent to see if it is still visible after switching MPI and Hadronisation on. As such two reasonable choices to analyse are the third jet transverse momentum and the soft third jet pseudorapidity spectrum, where we have seen clear coherent radiative suppression previously.

(a)   (b)
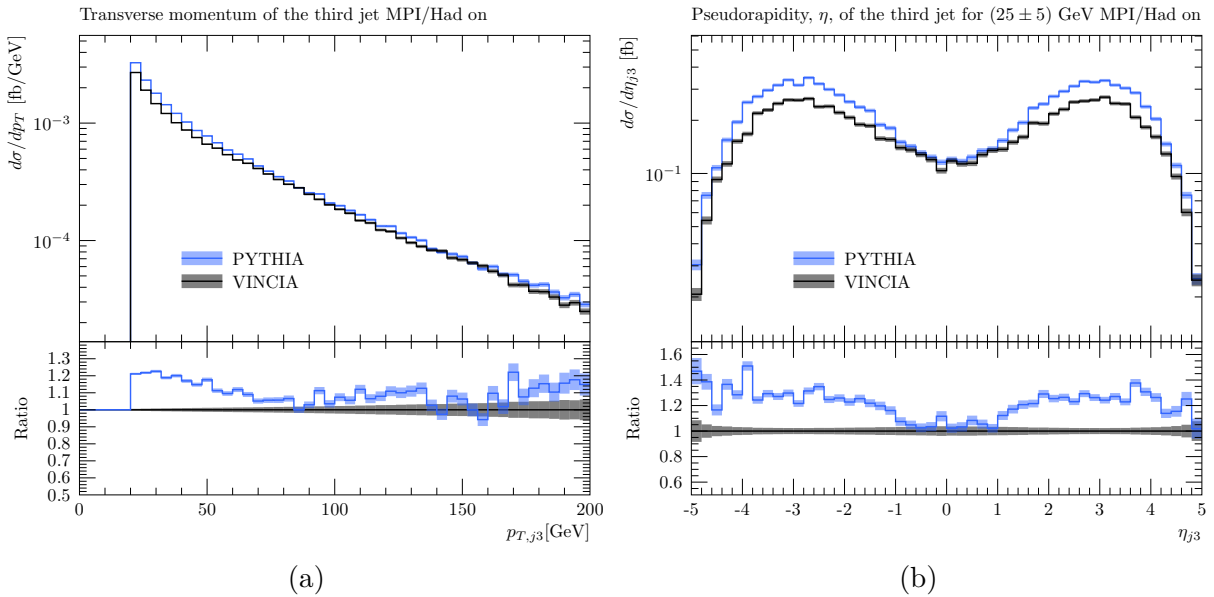
Figure 5.9: (Left) Transverse Momentum spectrum of the third jet with MPI and Hadronisation on (Right) Pseudorapidity spectrum of the third jet with MPI and Hadronisaiton on.

As can be seen in figure 5.9 the differences between PYTHIA and VINCIA are significantly reduced, though they do not vanish. We can see the effects of MPI filling up our distributions with somewhat incoherent radiation. Interestingly, the region of pseudorapidity closest to zero is most in agreement in terms of coherence with MPI and Hadronisation on, possibly indicating that we have hit the noise floor in this region - with a similar effect being present around 100 GeV for the transverse momentum histogram. Though these phenomenon are beyond the scope of this thesis the preliminary results are interesting and surprising, certainly not an effect we would expect to see; especially given that we appear to be *reducing* the cross section of our process for our the pseudorapidity histogram, an effect we would almost never expect to see from either MPI or Hadronisation.

Chapter 6

Final thoughts and Future work

My thesis has compared the PYTHIA and VINCIA showers extensively to determine the merits of generating coherent radiation using the DGLAP based, or inherently coherent antenna based, showers for WBF. By comparing the effects of observables such as p_t, η and H_T, on known coherent sensitive phenomena, such as the third jet, we find that the observed differences between these showers are substantial. PYTHIA greatly over-represents the amount of soft radiation in these events, particularly in low pseudorapidity regions of phase space where we expect the soft suppression to be at its greatest. Instead PYTHIA is predicting a large (and hence unphysical) amount of radiation - with up to a ≈ 10 times difference between it PYTHIA and VINCIA. By contrast VINCIA appears to be capturing the correct physics for WBF, with PYTHIAs under performance being in line with previous studies indicating that PYTHIAs treatment of radiation for WBF being inadequate [62].

As such we recommend an antenna or antenna-like treatment to simulate WBF, in particular such that the IF radiation from the born level of WBF is treated by a coherent formalism. VINCIA or PYTHIA with a dipole recoil appear to correctly capture the coherent physics of the process, while PYTHIAs simple shower by default does not. These effects also appear to be present in some form when considering Hadronisation and MPI effects, though we caution the reader to keep in context that these are merely preliminary results - and that stronger conclusions warrant further study.

On that remark, we believe our results point to interesting physics regarding the shower process for WBF in Monte Carlo Event Generators. If one wished to collect the main results of this thesis into a publishable state we would recommend replicating the analysis at the NLO+LL level, as opposed to LO+LL as is done here - as well as including further analysis into both the Hadronisation and MPI effects we see in our preliminary results. While the results from the LO+LL analysis are useful, as they point to interesting phenomenon, a typical analysis in the field would likely be done with the hard processes set at least at NLO (if not possibly NNLO). Since a larger portion of the phase space is covered by the NLO hard process we would expect that the PYTHIA and VINCIA showers would have smaller (or possibly even convergent) coherent differences compared to each over. Though we believe that these coherence effects go beyond NLO and as such will still be present to that level, albeit diminished.

References

[1] P. W. Higgs, "Broken Symmetries and the Masses of Gauge Bosons," *Physical Review Letters*, vol. 13, pp. 508–509, 1964.

[2] F. Englert and R. Brout, "Broken Symmetry and the Mass of Gauge Vector Mesons," *Physical Review Letters*, vol. 13, pp. 321–323, 1964.

[3] G. S. Guralnik *et al.*, "Global Conservation Laws and Massless Particles," *Physical Review Letters*, vol. 13, pp. 585–587, 1964.

[4] G. Aad *et al.*, "Observation of a new particle in the search for the Standard Model Higgs boson with the ATLAS detector at the LHC," *Physics Letters B*, vol. 716, no. 1, pp. 1–29, 2012.

[5] S. Chatrchyan *et al.*, "Observation of a new boson at a mass of 125 GeV with the CMS experiment at the LHC," *Physics Letters B*, vol. 716, no. 1, pp. 30–61, 2012.

[6] P. A. R. Ade *et al.*, "Planck 2013 results. I. Overview of products and scientific results," *Astronomy and Astrophysics*, vol. 571, 2014.

[7] R. S. Aspden, M. J. Padgett, and G. C. Spalding, "Video recording true single-photon double-slit interference," *American Journal of Physics*, vol. 84, no. 9, pp. 671–677, 2016.

[8] A. H. Tavabi, C. B. Boothroyd, E. Yücelen, S. Frabboni, G. C. Gazzadi, R. E. Dunin-Borkowski, and G. Pozzi, "The Young-Feynman controlled double-slit electron interference experiment," *Scientific Reports*, vol. 9, p. 10458, 2019.

[9] A. E. Chudakov, "On an ionization effect related to the observation of electron-positron pairs at very high energies," *Bulletin of the Academy of Sciences of the USSR. Physical Series*, vol. 19, no. 6, pp. 589–595, 1955.

[10] P. Z. Skands, "Introduction to Event Generators. Lecture 2: Parton Showers." 11th MCnet School, Lund Univeristy, 2017. School of Physics and Astronomy, Monash University.

[11] Y. Nagashima, *Elementary Particle Physics*, vol. 2, ch. 10.2. Wiley-VCH, 2013.

[12] M. Thomson, *Modern Particle Physics*. Cambridge University Press, 1 ed., 2013.

[13] R. Wolf, *The Higgs Boson Discovery at the Large Hadron Collider*. Springer Tracts in Modern Physics, 1 ed., 2015.

[14] M. Mangano, "LHC at 10: the physics legacy." arXiv preprint arXiv:2003.05976v1, 2020.

[15] ALEPH, "Precision Electroweak Measurements and Constraints on the Standard Model," Tech. Rep. CERN-PH-EP-2010-095, European Organization For Nuclear Research, 12 2010.

[16] "Search for the Standard Model Higgs boson at LEP," *Physics Letters B*, vol. 565, pp. 61–75, 2003.

[17] T. Aaltonen *et al.*, "Combination of Tevatron Searches for the Standard Model Higgs Boson in the W^+W^- Decay Mode," *Physical Review Letters*, vol. 104, p. 061802, 2010.

[18] T. Aaltonen *et al.*, "Evidence for a Particle Produced in Association with Weak Bosons and Decaying to a Bottom-Antibottom Quark Pair in Higgs Boson Searches at the Tevatron," *Physical Review Letters*, vol. 109, no. 7, 2012.

[19] J. Gao, L. Harland-Lang, and J. Rojo, "The structure of the proton in the LHC precision era," *Physics Reports*, vol. 742, pp. 1–121, 2018.

[20] "LHC Higgs Cross Section Working Group." https://twiki.cern.ch/twiki/bin/view /LHCPhysics/LHCHXSWG. Accessed: July 2020.

[21] H. M. Georgi, S. L. Glashow, M. E. Machacek, and D. V. Nanopoulos, "Higgs Bosons from Two-Gluon Annihilation in Proton-Proton Collisions," *Physical Review Letters*, vol. 40, pp. 692–694, 1978.

[22] V. Ravindran, J. Smith, and W. van Neerven, "NNLO Corrections to the Higgs Production Cross Section," *Nuclear Physics B - Proceedings Supplements*, vol. 135, pp. 35–40, 2004.

[23] R. Cahn and S. Dawson, "Production of very massive Higgs bosons," *Physics Letters B*, vol. 136, no. 3, pp. 196–200, 1984.

[24] V. D. Barger, K.-m. Cheung, T. Han, J. Ohnemus, and D. Zeppenfeld, "A Comparative study of the benefits of forward jet tagging in heavy Higgs production at the SSC," *Physical Review D*, vol. 44, pp. 1426–1437, 1991.

[25] G. Aad *et al.*, "Measurement of the electroweak production of dijets in association with a Z-boson and distributions sensitive to vector boson fusion in proton-proton collisions at $\sqrt{s} = 8$ TeV using the ATLAS detector," *Journal of High Energy Physics*, vol. 2014, no. 4, 2014.

[26] G. Aad *et al.*, "Measurements of Higgs Bosons Decaying to Bottom Quarks from Vector Boson Fusion Production with the ATLAS Experiment at $\sqrt{s} = 13$ TeV," 11 2020.

[27] J. Chang, K. Cheung, C.-T. Lu, and T.-C. Yuan, "WW scattering in the era of post-Higgs-boson discovery," *Physical Review D*, vol. 87, no. 9, 2013.

[28] J. M. Butterworth, A. R. Davison, M. Rubin, and G. P. Salam, "Jet Substructure as a New Higgs-Search Channel at the Large Hadron Collider," *Physical Review Letters*, vol. 100, no. 24, 2008.

[29] D. de Florian *et al.*, "Handbook of LHC Higgs CrossSections: 4. Deciphering the nature of the Higgs sector," *LHC Higgs Cross Section Working Group*, 2017.

[30] G. Aad *et al.*, "Identification of boosted Higgs bosons decaying into b-quark pairs with the ATLAS detector at 13 TeV," *The European Physical Journal C*, vol. 79, no. 10, 2019.

[31] M. Aaboud *et al.*, "Search for the Decay of the Higgs Boson to Charm Quarks with the ATLAS Experiment," *Physical Review Letters*, vol. 120, no. 21, 2018.

[32] M. Ritzmann, D. Kosower, and P. Skands, "Antenna showers with hadronic initial states," *Physics Letters B*, vol. 718, p. 1345–1350, Jan 2013.

[33] The ATLAS Collaboration, "The simulation principle and performance of the AT-LAS fast calorimeter simulation FastCaloSim," Tech. Rep. ATL-PHYS-PUB-2010-013, CERN, 2010.

[34] S. Chatrchyan *et al.*, "The CMS Experiment at the CERN LHC," *Journal of Instrumentation*, vol. 3, p. S08004, 2008.

[35] R. J. Cantrill, "Optimisation of VBF tagging for Higgs $\rightarrow \gamma\gamma$." IoP Conference, 2012.

[36] "Facts and figures about the LHC." Retrieved from URL https://home.cern/resources/faqs/facts-and-figures-about-lhc. Visited 14th June 2020.

[37] T. Sjöstrand, S. Ask, J. R. Christiansen, R. Corke, N. Desai, P. Ilten, S. Mrenna, S. Prestel, C. O. Rasmussen, and P. Z. Skands, "An introduction to pythia 8.2," *Computer Physics Communications*, vol. 191, p. 159–177, Jun 2015.

[38] M. Bähr *et al.*, "Herwig++ physics and manual," *The European Physical Journal C*, vol. 58, p. 639–707, Nov 2008.

[39] E. Bothmann *et al.*, "Event generation with sherpa 2.2," *SciPost Physics*, vol. 7, Sep 2019.

[40] J. C. Collins, D. E. Soper, and G. F. Sterman, "Factorization for Short Distance Hadron - Hadron Scattering," *Nuclear Physics B*, vol. 261, pp. 104–142, 1985.

[41] S. Frixione, P. Nason, and G. Ridolfi, "The powheg-hvq manual version 1.0," 2007.

[42] S. Frixione, F. Stoeckli, P. Torrielli, B. R. Webber, and C. D. White, "The mc@nlo 4.0 event generator." Preprint: 1010.0819, 2010.

[43] C. Duhr, "Qcd at nnlo and beyond," *Nuclear and Particle Physics Proceedings*, vol. 273-275, pp. 2128 – 2135, 2016. 37th International Conference on High Energy Physics (ICHEP).

[44] P. Bartalini and J. R. Gaunt, eds., *Multiple Parton Interactions at the LHC*, vol. 29. WSP, 2019.

[45] B. Andersson, G. Gustafson, G. Ingelman, and T. Sjöstrand, "Parton fragmentation and string dynamics," *Physics Reports*, vol. 97, no. 2, pp. 31–145, 1983.

[46] B. Andersson, *The Lund Model.* Cambridge Monographs on Particle Physics, Nuclear Physics and Cosmology, Cambridge University Press, 1998.

[47] D. Amati and G. Veneziano, "Preconfinement as a property of perturbative QCD," *Physics Letters B*, vol. 83, no. 1, pp. 87–92, 1979.

[48] R. Kleiss and H. Kuijf, "Multi - Gluon Cross-sections and Five Jet Production at Hadron Colliders," *Nuclear Physics B*, vol. 312, pp. 616–644, 1989.

[49] F. A. Dreyer and A. Karlberg, "Vector-boson fusion higgs production at three loops in qcd," *Physical Review Letters*, vol. 117, Aug 2016.

[50] G. Altarelli and G. Parisi, "Asymptotic freedom in parton language," *Nuclear Physics B*, vol. 126, no. 2, pp. 298–318, 1977.

[51] Y. L. Dokshitzer, "Calculation of the Structure Functions for Deep Inelastic Scattering and e^+ e^- Annihilation by Perturbation Theory in Quantum Chromodynamics.," *Soviet Physics, Journal of Experimental and Theoretical Physic*, vol. 46, pp. 641–653, 1977.

[52] V. Gribov and L. Lipatov, "Deep inelastic e p scattering in perturbation theory," *Soviet Journal of Nuclear Physics*, vol. 15, pp. 438–450, 1972.

[53] S. Höche, "Introduction to parton-shower event generators." Preprint: 1411.4085, 2014.

[54] P. Skands, "Introduction to QCD." Preprint: 1207.2389, 2017.

[55] V. V. Sudakov, "Vertex Parts at Very High Energies in Quantum Electrodynamics," *Soviet Physics, Journal of Theortical Physics*, vol. 30, pp. 87–95, 1956.

[56] T. Sjöstrand and P. Z. Skands, "Transverse-momentum-ordered showers and interleaved multiple interactions," *The European Physical Journal C*, vol. 39, no. 2, pp. 129–154, 2005.

[57] G. Marchesini and B. Webber, "Simulation of QCD jets including soft gluon, interference," *Nuclear Physics B*, vol. 238, no. 1, pp. 1–29, 1984.

[58] M. Delmastro, "Experimental Particle Physics: 1. units, quantities, kinematics, measurements." European Scientific Institute - Archamps, 2014.

[59] M. Cacciari, G. P. Salam, and G. Soyez, "Fastjet user manual," *The European Physical Journal C*, vol. 72, Mar 2012.

[60] M. Cacciari, G. P. Salam, and G. Soyez, "The anti-ktjet clustering algorithm," *Journal of High Energy Physics*, vol. 2008, p. 063–063, Apr 2008.

[61] B. Cabouat and T. Sjöstrand, "Some dipole shower studies," *The European Physical Journal C*, vol. 78, Mar 2018.

[62] B. Jäger, A. Karlberg, S. Plätzer, J. Scheller, and M. Zaro, "Parton-shower effects in higgs production via vector-boson fusion," *The European Physical Journal C*, vol. 80, Aug 2020.

[63] F. James, "Monte Carlo Theory and Practice," *Reports on Progress in Physics*, vol. 43, no. 9, pp. 1145–1189, 1980.

[64] M Tanabashi and others, "Review of particle physics: Particle data group - chapter 40. monte carlo techniques," *Physical Review D*, vol. 98, no. 3, pp. 542–545, 2018.

Appendix A

Monte Carlo Integration

The reader may be interested what the so called "Monte Carlo" (MC) method actually is, of which this appendix hopes to address. The MC method is a name given to any process that utilities MC integration. This technique of integration utilities random numbers[1] to perform a numerical integration (see appendix B for a basic proof of this method of integration). This is done by sampling, either flatly or by some functional dependence, a random distribution of numbers in the volume of integration, which leads to a numerical solution of the integral. This solution becomes more accurate for a larger number of samplings, with the caveat that there is some probability, P, that this convergence will fail.

One might ask why we would want to use Monte Carlo integration with its risk of failure, when other techniques for numerical integration, such as the trapezoid rule, which do not have this flaw. The answer comes down to the rate of convergence (which is related to the uncertainty) in high dimensions. For a small number of dimensions MC integration converges slower than most numerical methods on integration, however the convergence of MC integration is independent of the dimensionality of the integral, while other numerical methods generally have better convergence rate for additional dimensions. This relationship is demonstrated in the table below:

Relative uncertainty after n evaluations	Convergence rate in one dimensions	Convergence rate in d dimensions
Monte Carlo	$n^{-1/2}$	$n^{-1/2}$
Trapezoidal rule	n^{-2}	$n^{-2/d}$
Simpson's rule	n^{-4}	$n^{-4/d}$
Gauss rule	n^{-2m+1}	$n^{(-2m+1)/d}$

Table A.1: The relative uncertainty (proportional to the convergence rate) of various numerical integration techniques in 1 and d dimensions. As can be seen, for small d Monte Carlo is an inefficient method of numerical integration, while for large d the Monte Carlo method is much faster then other numerical methods [63].

In experiments at the LHC typically create on the order of $\mathcal{O}(100) - \mathcal{O}(1000)$ particles [53]. Each of these particles adds with it three dimensions to the phase space of the process. As such we quickly enter the regime where MC integration is far superior than

---

[1]Or in practice pseudrandom numbers

other numerical methods, even including the possibility of the failure of convergence. This is true even when calculating just the hard sub-process, where the number of outgoing particles is far smaller the dimensionality of the phase space still leads us to use MC integration. Furthermore MC integration of the hard process can be used to start a Monte Carlo Markov Chain (MCMC), which is the bases of the shower process, which is discussed further in section 3.2.

Appendix B

Proof for the Monte Carlo Method of Integration

To begin we have the numerical integral of some n-dimensional function f(x) of:

$$I = \int_V f(x) d^n x, \tag{B.1}$$

where V is some arbitrary n-dimensional volume in real space. Sampling N uniformly randomly distributed points in V by the law of large numbers and the central limit theorem we have:

$$I \simeq Q_n = \frac{V}{N} \sum_{i=1}^{N} f(x_i) = \langle f \rangle, \tag{B.2}$$

where by the law of large numbers we have that:

$$lim_{N \to \infty} Q_N = I \tag{B.3}$$

Now the estimated error of our integral is summarised by the square root of it's variance, namely:

$$\sigma_{Q_n} = \sqrt{Var(Q_n)} = \sqrt{\langle Q_n^2 \rangle - \langle Q_n \rangle^2}. \tag{B.4}$$

Which in terms of the variance of our original function f(x) is:

$$\sigma_{Q_n} = \sqrt{\frac{V^2}{N^2} \sum_{i=1}^{N} Var(f)}. \tag{B.5}$$

Which becomes:

$$\sigma_{Q_n} = \sqrt{\frac{V^2}{N} Var(f)}. \tag{B.6}$$

Which finally simplifies to:

$$\sigma_{Q_n} = V \sqrt{\frac{Var(f)}{N}}. \tag{B.7}$$

As can be seen in the limit as $N \to \infty$ the error in our approximation goes to 0; most importantly this error is independent of the number of dimensions of our integral.

This subtlety here is that while in calculus we have that $\{A\}$ will converge to B if n exists for which $|A_{i>n} - B| < \epsilon$ for any $\epsilon > 0$, we must treat the Monte Carlo convergence statistically. As such instead we have that $\{A\}$ converges to B if n exists for which the

probability for $|A_{i>n} - B| < \epsilon$ is greater than P for any $P \in [0, 1]$ and for any $\epsilon > 0$. As such we always have the chance of our convergence failing [63].

The second subtlety is that we have chosen a flat distribution to randomly sample from. While the proof still applies to a non-flat random distribution a careful examination of different possible distributions can lead to a low error/faster convergence rate (see [64] for more insight into this).

Appendix C

Sudakov Veto Algorithm

For the Sudakov veto Algorithm we have that:

$$R = exp(-\int_{t_1}^{t_0} dt \hat{f}(t)) = \hat{\Delta}(t_0, t_1), \tag{C.1}$$

for some $\hat{f}(t) > f(t)$ for all t and some uniformly distributed random number $R \in [0, 1]$, which is accepted with probability:

$$P_{acc}(t) = \frac{f(t)}{\hat{f}(t)}. \tag{C.2}$$

Now we want to prove that this is equivalent to $R = \delta(t_0, t_1) = exp(-\int_{t_1}^{t_0} dt f(t))$. To do this let's consider the probability that a branching will occur at time t_1. If there have been no rejected trials before this time the probability is given by:

$$\mathcal{P}_0 = \hat{\Delta}(t_0, t_1)\hat{f}(t_1)P_{acc}(t_1), \tag{C.3}$$

which since $P_{acc}(t) = \frac{f(t)}{\hat{f}(t)}$ we can simplify to:

$$\mathcal{P}_0 = \hat{\Delta}(t_0, t_1)f(t_1). \tag{C.4}$$

What about the case if one intermediate time has been rejected? If we have rejected one trial at time t_1, with the next accepted trail now being t_2 the probability then becomes:

$$\mathcal{P}_1 = \int_{t_2}^{t_1} dt_1 \hat{f}(t_1)(1 - P_{acc}(t_1))\hat{\Delta}(t_0, t_1)\hat{\Delta}(t_1, t_2). \tag{C.5}$$

Which can be simplified to:

$$\mathcal{P}_1 = \mathcal{P}_0 \int_{t_2}^{t_0} dt_1(\hat{f}(t_1) - f(t_1)). \tag{C.6}$$

What about the case where two rejected branchings have occurred before? In this case we have:

$$\mathcal{P}_2 = \mathcal{P}_0 \int_{t_3}^{t_0} dt_1(\hat{f}(t_1) - f(t_1)) \int_{t_3}^{t_1} dt_2(\hat{f}(t_2) - f(t_2)) \tag{C.7}$$

Here we can use the fact that $\int_a^b dx f(x) \int_a^c dy f(y) = \frac{1}{2}(\int_a^b f(x))^2$ to simplify this to:

$$\mathcal{P}_2 = \frac{1}{2}\mathcal{P}_0(\int_{t_3}^{t_0} dt_1(\hat{f}(t_1) - f(t_1)))^2 \tag{C.8}$$

The identity just used is due to the fact that the double integral is a triangular integral with factorised integrand which is symmetric under the interchange of the integration variables. For n higher terms we thus have a n-dimensional hyper-triangle, we can reduce these n-dimensional hyper triangles just as with the regular triangle, with a pre-factor of $\frac{1}{n!}$. Thus the probability to accept time t in any step becomes:

$$\mathcal{P}(t) = \sum_{n=0}^{\infty} \mathcal{P}_n(t) = \mathcal{P}_0(t) \sum_{n=1}^{\infty} \frac{1}{n!} (\int_t^{t_0} dt'(\hat{f}(t') - f(t')))^n. \tag{C.9}$$

Which using $exp(x) = \sum_{i=0}^{\infty} \frac{1}{i!} x^i$ we have:

$$\mathcal{P}(t) = f(t)exp(-\int_t^{t_0} dt' f(t')) \tag{C.10}$$

Which is the probability to generate an event at time t with no emission between t_0 and t. This is identical to the form if we had not used the veto algorithm, and as such proves the correctness of the veto algorithm.

Appendix D

Angular Ordering

We can prove why the angular ordering approach reconstructs azimuthally averaged behaviour with DGLAP splitting kernels by first considering the soft Eikonal factor multiplied by E_j^2:

$$E_j^2 \frac{(p_i \cdot p_k)}{(p_i \cdot p_j)(p_j \cdot p_k)}, \tag{D.1}$$

where i is the mother parton, j is the radiated gluon and k is the recoiled parton. We can write out our 4-products in terms of the angles between the particles in the high energy limit (where $E \gg m$) as:

$$\frac{1 - cos\theta_{ik}}{(1 - cos\theta_{ij})(1 - cos\theta_{jk})} = \frac{1 - cos\theta_{ik}}{(1 - cos\theta_{ij})(1 - cos\theta_{jk})} \pm \frac{1}{2(1 - cos\theta_{ij})} \mp \frac{1}{2(1 - cos\theta_{jk})}, \tag{D.2}$$

where on the right hand side we have isolated the ij and ik collinear pieces. Now considering only the ij piece let's integrate over the azimuthal angle ϕ_{ij}:

$$\int_0^{2\pi} \frac{d\phi_{ij}}{4\pi} \frac{1 - cos\theta_{ik}}{(1 - cos\theta_{ij})(1 - cos\theta_{jk})} + \frac{1}{1 - cos\theta_{ij}} - \frac{1}{1 - cos\theta_{jk}} = \frac{1}{2(1 - cos\theta_{ij})}(1 + \frac{cos\theta_{ij} - cos\theta_{ik}}{|cos\theta_{ij} - cos\theta_{ik}|}). \tag{D.3}$$

Looking closely we see that the fraction $1 + \frac{cos\theta_{ij} - cos\theta_{ik}}{|cos\theta_{ij} - cos\theta_{ik}|}$ equals 2 if $\theta_{ij} > \theta_{ik}$ and 0 if $\theta_{ij} < \theta_{ik}$. As such by setting soft gluon radiation to be $\frac{1}{1 - cos\theta_{ij}}$ for $\theta_{ij} > \theta_{ik}$ and 0 for $\theta_{ij} < \theta_{ik}$ we reconstruct the azimuthally averaged soft coherence previously lost.